



## OPEN ACCESS

## EDITED BY

Shujuan Zhang,  
Nanjing University, China

## REVIEWED BY

Katarzyna Pawluk,  
Warsaw University of Life Sciences, Poland  
Bingding Wu,  
Suzhou University of Science and Technology,  
China

## \*CORRESPONDENCE

Jane Liu,  
✉ janejj.liu@utoronto.ca

RECEIVED 27 March 2025

ACCEPTED 19 May 2025

PUBLISHED 03 July 2025

## CITATION

Zang Z, Liu J, Ge E and Zhang Y (2025) Two-decade spatiotemporal variations in ground-level ozone over Ontario, Canada. *Front. Environ. Eng.* 4:1601213.  
doi: 10.3389/fenve.2025.1601213

## COPYRIGHT

© 2025 Zang, Liu, Ge and Zhang. This is an open-access article distributed under the terms of the [Creative Commons Attribution License \(CC BY\)](#). The use, distribution or reproduction in other forums is permitted, provided the original author(s) and the copyright owner(s) are credited and that the original publication in this journal is cited, in accordance with accepted academic practice. No use, distribution or reproduction is permitted which does not comply with these terms.

# Two-decade spatiotemporal variations in ground-level ozone over Ontario, Canada

Zhou Zang<sup>1</sup>, Jane Liu<sup>1\*</sup>, Erjia Ge<sup>2</sup> and Yi Zhang<sup>1</sup>

<sup>1</sup>Department of Geography and Planning, University of Toronto, Toronto, ON, Canada, <sup>2</sup>Dalla Lana School of Public Health, University of Toronto, Toronto, ON, Canada

**Introduction:** Ground-level ozone ( $O_3$ ) remains a persistent air quality concern in Ontario, Canada's most populous province. Understanding long-term trends and spatially explicit details of  $O_3$  is important for supporting air quality management in Ontario.

**Method:** We construct a high-resolution (daily, 10 km) dataset of maximum daily 8-hour average  $O_3$  (MDA8  $O_3$ ) over Ontario from 2004 to 2023, through a two-step machine learning model. The model has incorporated our hypothesis that accounting for transboundary influences can enhance the accuracy of  $O_3$  estimation.

**Results:** Validation against *in-situ* measurements confirms the hypothesized high accuracy of the dataset ( $R^2 = 0.82$ , RMSE = 4.99 ppb), outperforming the traditional model and two existing datasets. The dataset reveals pronounced spatiotemporal heterogeneity in MDA8  $O_3$  concentrations, which are low in northern Ontario but high in southern Ontario, especially in southwest Ontario. Seasonally, the provincial mean MDA8  $O_3$  peaks in spring (~40 ppb) and dips in autumn (~27 ppb), while spatial MDA8  $O_3$  in summer is most heterogeneous among all seasons, with a peak in southwestern Ontario. From 2004 to 2023, the provincial mean MDA8  $O_3$  shows no significant trend, while a significant decreasing trend (~0.1 ppb/year,  $p < 0.05$ ) appears in southern Ontario, where MDA8  $O_3$  increases in winter but decreases in summer, both significantly. The number of days exceeding the World Health Organization (WHO)  $O_3$  guideline range from 10 to 80 days in southern Ontario, with a decline of 1–4 days (up to 15%) per year over 2004–2023.

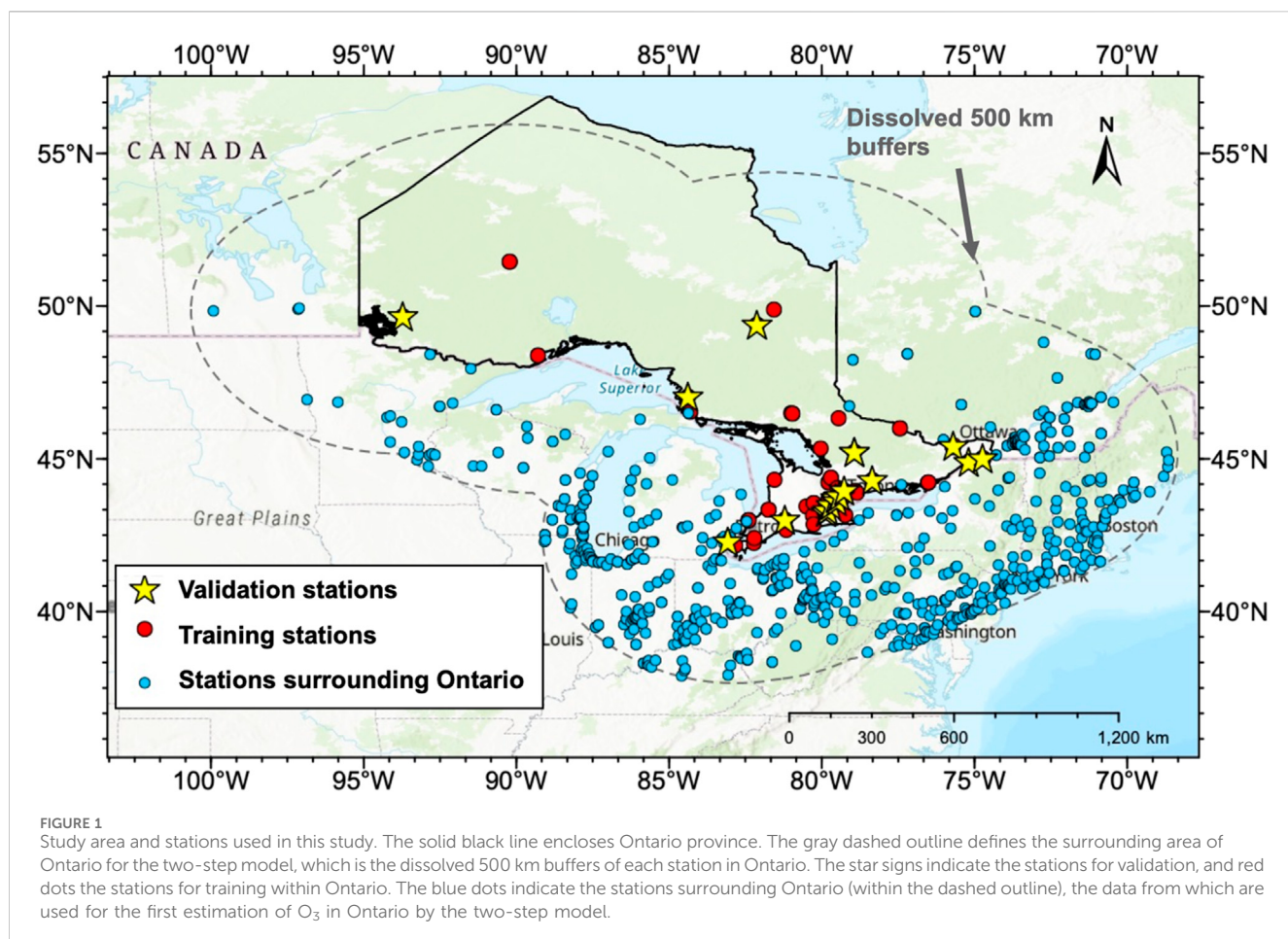
**Discussion:** The analysis suggests that  $O_3$  in southern Ontario is impacted by both anthropogenic emissions and meteorology. Reductions in  $O_3$  precursor emissions have effectively lowered summertime  $O_3$  across southern Ontario, partially offsetting the meteorological-driven increase in  $O_3$ . This MDA8  $O_3$  dataset offers a valuable resource for further research in environmental health, air quality policy, and  $O_3$  impact on agriculture.

## KEYWORDS

ground-level ozone, air pollution, spatiotemporal variations, high resolution, machine learning, Ontario

## 1 Introduction

Ground-level ozone ( $O_3$ ) is a major air pollutant with well-documented adverse effects on human health, ecosystems and agriculture (Fleming et al., 2018; Mills et al., 2018). Although  $O_3$  concentrations in Canada are generally low (WHO, 2023), hourly  $O_3$  concentrations in Ontario (Figure 1), the most populated and urbanized province in



Canada, still can be higher than 80 ppb, which is the Ambient Air Quality Criterion (AAQC), particularly in warmer seasons over southern Ontario (Ministry of the Environment and Climate Change, 2022). Continuous monitoring of ground-level O<sub>3</sub> is, therefore, important to supporting air quality management, especially in the populated areas like southern Ontario. The National Air Pollution Surveillance Program (NAPS) has collected hourly ground-level O<sub>3</sub> measurements under a consistent standard protocol since 1969 (<https://www.canada.ca/en/environment-climate-change/services/air-pollution/monitoring-networks-data/national-air-pollution-program.html>). Based on 39 air monitoring stations in the NAPS program, the Air Quality in Ontario Report show that O<sub>3</sub> pollution during the warm seasons is still an important environmental issue in southwestern Ontario (Ministry of the Environment and Climate Change, 2018a; Ministry of the Environment and Climate Change, 2018b; Ministry of the Environment and Climate Change, 2018c; Ministry of the Environment and Climate Change, 2019; Ministry of the Environment and Climate Change, 2020; Ministry of the Environment and Climate Change, 2021; Ministry of the Environment and Climate Change, 2022). However, the limited numbers and sparsely distribution of monitoring stations across Ontario can introduce substantial geographical bias, restricting the ability to analyze detailed spatial and temporal patterns of ozone (Schultz et al., 2017). As a result, comprehensive assessments of O<sub>3</sub>

variability and long-term trends across the province remain limited. In addition, data from sparsely distributed monitoring stations cannot satisfy requirements for studying impact of O<sub>3</sub> pollution on crop yields and O<sub>3</sub>-health implications, because spatially explicit and seamless data over large areas are generally needed for these studies.

To address this research gap, it is highly desirable to construct a spatially explicit and long-term dataset of ground-level O<sub>3</sub>. However, existing ground-level O<sub>3</sub> datasets for Ontario are confined by their large uncertainties, limited spatial resolution or temporal coverage. While satellite remote sensing has been widely used for air quality monitoring, current retrieval techniques typically provide the total column ozone, tropospheric ozone, or vertical ozone profiles at different vertical ranges (Liu et al., 2010), which do not directly correspond to the ground-level concentrations (Bai et al., 2016). Because ground-level O<sub>3</sub> represents only a small fraction of total column ozone, retrievals based on ultraviolet measurements often have large uncertainties due to limited sensitivity near the ground (Bhartia, 2002). Moreover, satellite records are often short in duration and vary across instruments, and merging these datasets can introduce additional uncertainties (Rahpoe et al., 2015). Chemical transport models (CTMs) can simulate long-term and spatially explicit O<sub>3</sub> fields, but they are also subject to limitations. Notably, large uncertainties remain in simulating O<sub>3</sub> responses to nitrogen oxides (NO<sub>x</sub>) emissions, leading

to mismatches in magnitude and trends when compared to observations (Miyazaki et al., 2020). Additionally, the spatial resolutions of most CTMs are comparatively coarse (typically  $>0.5^{\circ}$ ), which limits their utility for exposure assessments on local and regional scales, especially for health and agriculture applications. To improve the accuracy and spatiotemporal continuity of  $O_3$ , statistical models are also widely applied based on the relationship between  $O_3$  and the environmental factors as well as the sources of the precursor emissions. However, to date, a long-term  $O_3$  dataset with fine spatiotemporal resolutions based on statistical models are still unavailable for Ontario. Several studies have provided the global estimations which covers Ontario (Delang et al., 2021; Liu et al., 2023; Wang et al., 2025). However, these datasets are either covering too short periods ( $<5$  years) or with too coarse temporal resolutions (monthly or yearly).

In recent years, machine learning techniques have become preferred statistical algorithms for capturing the nonlinear relationship between  $O_3$  and various factors at regional and global scales (Zang et al., 2021; Chen et al., 2023; Yan et al., 2023). However, machine learning models rely heavily on the density and distributions of *in-situ* observation stations. In regions distant from any *in-situ* stations, model predictions could exhibit large modelling errors (Li et al., 2021; Wang et al., 2021). To address this issue, some models, such as linear mixed model (Lee et al., 2011) and geographically weighted regression (Ma et al., 2014), have been used to account for spatial heterogeneity in modelling relationships. However, these models usually assume a linear relationship, limiting their ability at capturing the nonlinear relationships. To overcome this, Li et al. (2021) proposed a locally weighted neural network constrained by global training. However, this approach may face challenges when only short-term *in-situ* measurements are available, as building a robust global model is difficult. They suggested leveraging data from other regions or time periods to enhance the model robustness. Similar to this idea, Yan et al. (2024) used latent information in grid cells without corresponding *in-situ* stations to improve the modelling performance over regions with sparse *in-situ* stations. Despite being effective, the computational cost for those statistical models can become unaffordable when the models are applied at fine resolutions. Liu et al. (2022) incorporated the co-located  $PM_{10}$  stations to enhance the spatiotemporal representativeness and accuracy of  $PM_{2.5}$  estimations, compromising between leveraging additional information and maintaining computational efficiency.

Here to enable investigation of spatiotemporal variations of  $O_3$  across Ontario, in the first step, we construct a ground-level  $O_3$  dataset over Ontario for two decades (2004–2023) with high accuracy. We select the “maximum daily 8-h average  $O_3$  (MDA8  $O_3$ )” for this dataset because this is one of the metrics that the World Health Organization (WHO) defines to assess air quality impact on health. To this end, we develop a new statistical model for MDA8  $O_3$  estimation using machine learning techniques. Technically, we use the *in-situ* stations inside and surrounding Ontario, as well as the data of adjacent grids and time windows from gridded data in our statistical model to fully exploit the information. We validate this dataset with *in-situ* measurements and compare this dataset with the one from traditional modelling, as well as the existing MDA8  $O_3$  datasets over Ontario. In the second step, based on the constructed MDA8  $O_3$  dataset, we analyze the

spatial and temporal variations of MDA8  $O_3$  concentrations across Ontario, showing the trends in response to the meteorological conditions and emission controls over the past two decades. We also assess the  $O_3$  pollution in Ontario following the WHO air quality guidelines. We expect to reveal the spatially explicit seasonality and trend in MDA8  $O_3$  across Ontario with more details than station data. The developed two-step model provides a novel approach for air pollution modelling, and the MDA8  $O_3$  dataset can support investigating health and agricultural implications of air quality in the future.

In proximity of the United States of America (USA), air quality in Ontario has been found to be largely influenced by transboundary transport of PM,  $O_3$ , and other pollutants from USA (Brook et al., 2002; Johnson et al., 2007; Liu and Cui, 2014; Ministry of the Environment and Climate Change, 2018b). Inspired by previous studies on air quality in Ontario and statistical model development, we make a hypothesis that employing the  $O_3$  data from stations surrounding Ontario in eastern USA, the transboundary influences from eastern USA on surface  $O_3$  in Ontario can be considered and the modelling accuracy can be enhanced. Specifically, we take advantage of the dense  $O_3$  *in-situ* monitoring stations in Ontario and surrounding areas in the USA to construct a surface MDA8  $O_3$  dataset over Ontario at daily temporal resolution and  $0.1^{\circ}$  horizontal resolution.

## 2 Materials and methods

### 2.1 Input data

**Table 1** shows the input data for constructing the MDA8  $O_3$  dataset. The *in-situ* measurements are processed into daily MDA8  $O_3$  concentrations, in unit of ppb. To unify the spatiotemporal resolution, all the gridded input data are resampled into the spatial resolution of  $0.1^{\circ}$  ( $\sim 10$  km), and all the hourly data are averaged into the daily mean.

#### 2.1.1 *In-situ* measurement

The *in-situ*  $O_3$  measurements over Canada and USA are used for the model development and evaluation. For Canada, hourly *in-situ*  $O_3$  measurements during 2004–2023 are acquired from the Environment and Climate Change Canada Data (ECCC) Catalogue, provided by the NAPS Program (<https://data-donnees.az.ec.gc.ca/data/air/monitor/national-air-pollution-surveillance-naps-program/Data-Donnees/>). In addition, 8-h average *in-situ* ozone data during 2004–2023 are acquired from United States Environmental Protection Agency (EPA) ([https://aqs.epa.gov/aqsweb/airdata/download\\_files.html](https://aqs.epa.gov/aqsweb/airdata/download_files.html)). The *in-situ* ozone data are processed into MDA8  $O_3$  concentrations for every station, according to the Ozone National Ambient Air Quality Standards (NAAQS, <https://www.epa.gov/criteria-air-pollutants/naaqs-table>).

#### 2.1.2 Reanalysis ozone and precursor data

Reanalysis data benefit the ozone modelling because they combine both model- and observation-based information to provide physically consistent data with continuous spatial and temporal coverage. Here, the surface ozone concentrations from three reanalysis datasets are evaluated: the European Centre for

TABLE 1 Data used for constructing the MDA8 O<sub>3</sub> dataset in this study.

Dataset name	Variable	Unit	Temporal resolution	Spatial resolution	Data source
Hourly ozone monitoring	O <sub>3</sub>	ppb	1-h	—	NAPS
8-Hour Average Data	O <sub>3</sub>	ppm	1-h	—	USA EPA
ERA5 Land	2m air temperature (T)	K	1-h	0.1° × 0.1°	Muñoz-Sabater et al. (2021)
	Surface air pressure (Ps)	Pa			
	2m dew point temperature	K			
	10m wind speed (WS)	m/s			
	Mean surface downward short-wave radiation flux (Fdir)	W/m <sup>2</sup>			
ERA5 single	Boundary layer height (BLH)	m	1-h	0.25° × 0.25°	Hersbach et al. (2020)
EAC4	Ozone mass mixing ratio (O <sub>3</sub> <sub>EAC4</sub> )	kg/kg	3-h	0.75° × 0.75°	Inness et al. (2019)
	Hydroxyl radical (OH)				
	Nitrogen dioxide (NO <sub>2</sub> )				
	Nitrogen monoxide (NO)				
	Formaldehyde (HCHO)				
MODIS	MCD12C1 land use type (LUT)	—	1-year	0.05° × 0.05°	Friedl and Sulla-Menashe (2022)
	MCD13C1 NDVI	—	16-day	0.05° × 0.05°	Didan (2021)
GPWv4	Population density (POP)	Persons/km <sup>2</sup>	5-year	0.008° × 0.008°	Center For International Earth Science Information Network-CIESIN-Columbia University (2017)

Medium-Range Weather Forecasts (ECMWF) reanalysis version 5 (ERA5), the Modern-Era Retrospective analysis for Research and Applications, Version 2 (MERRA-2), and ECMWF Atmospheric Composition Reanalysis 4 (EAC4). All three reanalysis datasets are processed into the daily mean with 0.1° spatial resolution to compare with *in-situ* ozone measurements. Figure 2 shows that EAC4 O<sub>3</sub> has the best agreement with *in-situ* data, with a coefficient of determination ( $R^2$ ) of 0.53 and a root-mean-square error (RMSE) of 29.54 ppb. MERRA-2 performs secondarily ( $R^2 = 0.23$ , RMSE = 34.77 ppb), while ERA5 is with the lowest accuracy ( $R^2 = 0.02$ , RMSE = 44.50 ppb). This is because only EAC4 data include a chemical transport model and consider chemical production and loss of tropospheric O<sub>3</sub> (Vieira et al., 2023), which better captures tropospheric chemistry and ozone dynamics. Therefore, the most accurate EAC4 O<sub>3</sub> data are employed in this study. In addition, O<sub>3</sub> precursors, including HCHO, hydroxyl radical, nitrogen dioxide and nitrogen monoxide from EAC4 are also used to improve the modelling accuracy.

### 2.1.3 Meteorological data

The formation and life span of surface O<sub>3</sub> are closely related to meteorological variables such as solar radiation, temperature, humidity, surface pressure, wind speed and boundary layer height (Agudelo-Castaneda et al., 2014; Khiem et al., 2010; Shen and Mickley, 2017; Hanes et al., 2019). Therefore, these six meteorological variables from ERA5-land are used to enhance the modelling accuracy (Table 1). The high spatial (0.1°) resolution of

ERA5 land data also help constrain the spatial resolution of O<sub>3</sub> estimations (Muñoz-Sabater et al., 2021).

### 2.1.4 Ancillary data

Vegetation and land cover are effective for improving the modelling accuracy, due to their significant association with the spatial distribution of O<sub>3</sub> (Wei et al., 2021; Zang et al., 2021). Here, ancillary inputs are considered including the normalized differential vegetation index (NDVI) and land use from the moderate resolution imaging spectroradiometer (MODIS), and population density from the Gridded Population of World Version 4 (GPWv4).

## 2.2 The two-step modelling

To fully take advantage of the *in-situ* measurements surrounding Ontario, a two-step model is developed to build the spatiotemporal relationship between *in-situ* MDA8 O<sub>3</sub> and multi-source predictors. In step 1, the *in-situ* measurements surrounding Ontario is used to provide an initial estimation for Ontario MDA8 O<sub>3</sub>. In step 2, the initial estimation is combined with *in-situ* measurements within Ontario to provide a final estimation of spatial-resolved MDA8 O<sub>3</sub> data across Ontario. In addition, the data from the adjacent grid points (8 grids) and time windows ( $\pm 1$  day) for each grid are used in both steps of modelling to fully exploit the information from gridded data. Only the most adjacent grid and time windows are selected here to ensure an acceptable

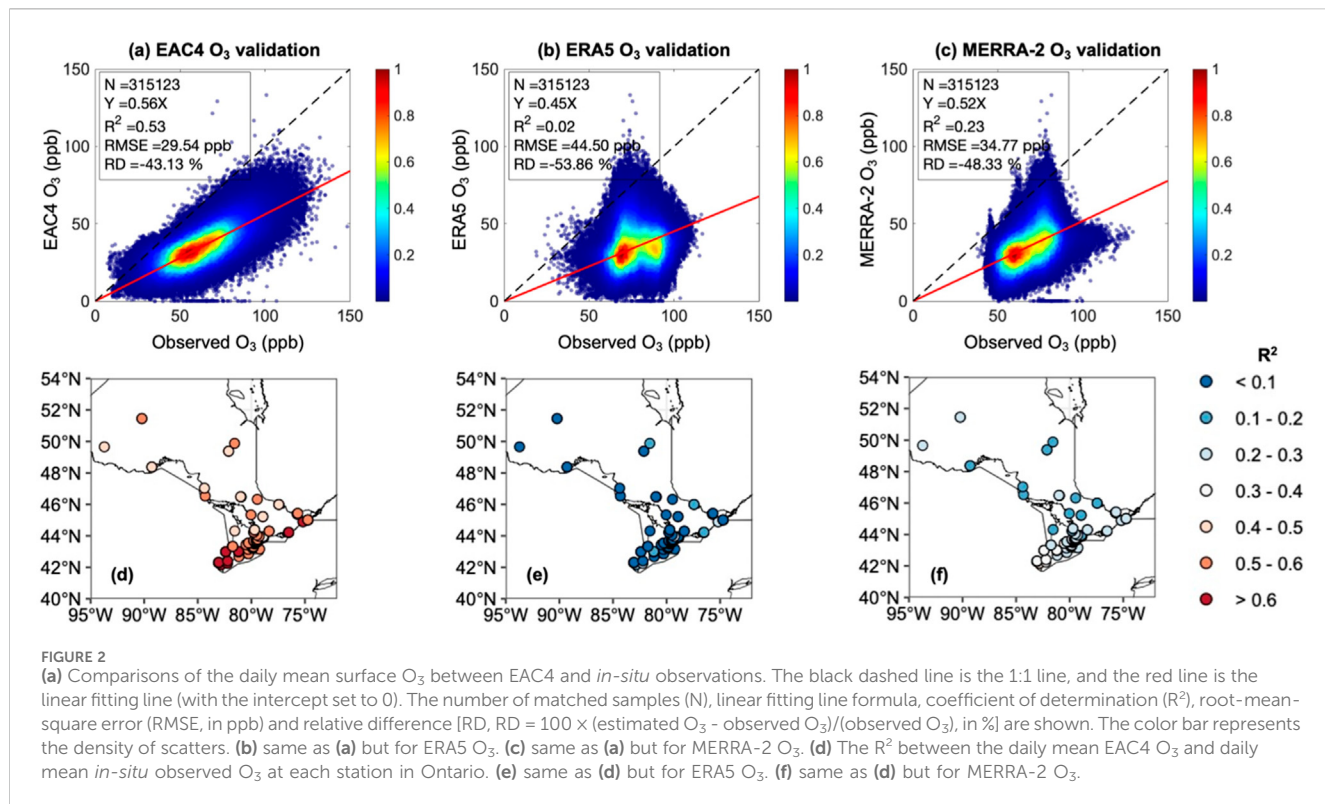


FIGURE 2

(a) Comparisons of the daily mean surface O<sub>3</sub> between EAC4 and *in-situ* observations. The black dashed line is the 1:1 line, and the red line is the linear fitting line (with the intercept set to 0). The number of matched samples (N), linear fitting line formula, coefficient of determination (R<sup>2</sup>), root-mean-square error (RMSE, in ppb) and relative difference [RD, RD = 100 × (estimated O<sub>3</sub> - observed O<sub>3</sub>)/(observed O<sub>3</sub>), %] are shown. The color bar represents the density of scatters. (b) same as (a) but for ERA5 O<sub>3</sub>. (c) same as (a) but for MERRA-2 O<sub>3</sub>. (d) The R<sup>2</sup> between the daily mean EAC4 O<sub>3</sub> and daily mean *in-situ* observed O<sub>3</sub> at each station in Ontario. (e) same as (d) but for ERA5 O<sub>3</sub>. (f) same as (d) but for MERRA-2 O<sub>3</sub>.

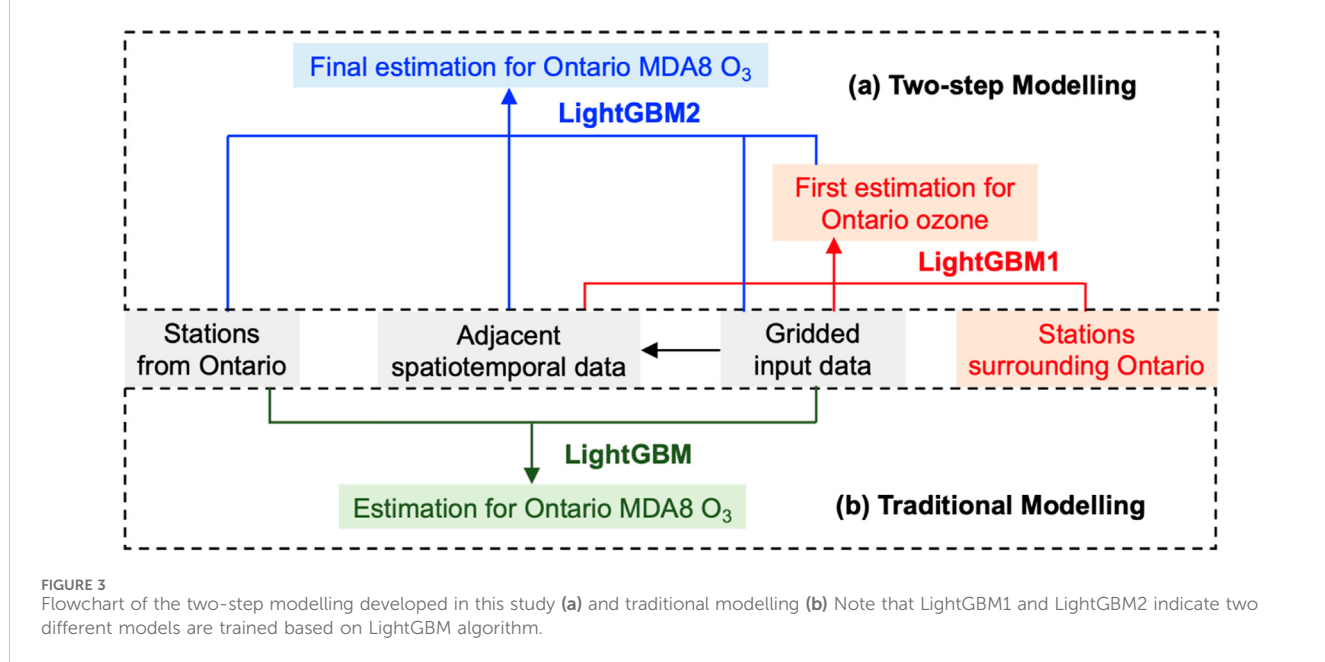


FIGURE 3

Flowchart of the two-step modelling developed in this study (a) and traditional modelling (b). Note that LightGBM1 and LightGBM2 indicate two different models are trained based on LightGBM algorithm.

computational time. Both steps use Light Gradient-Boosting Machine (LightGBM) algorithm to build the model, owing to its faster computation speed, lower memory consumption and capability of handling big data (Wei et al., 2021).

Figure 3a shows a detailed framework of this two-step modelling. In step 1, the data from the stations surrounding Ontario (blue stations in Figure 1) are used to provide a reliable estimated Ontario MDA8 O<sub>3</sub>

as a new predictor for step 2. To define the surrounding stations, a buffer of 500 km is generated for each station in Ontario (the gray dashed circle in Figure 1). Here, the 500 km buffer is determined by the most conservative ozone correlation length (500–1,000 km) in the troposphere, within which ozone concentrations are considered being significantly correlated (Liu et al., 2009). Therefore, for each station in Ontario, the stations within the radius of 500 km outside Ontario can be

determined as its surrounding stations. By merging all the radius of 500 km for each station in Ontario, the stations outside Ontario but within this buffer are considered as the surrounding stations. Step 2 is similar to traditional modelling (Figure 3b), yet with an additional predictor from the estimated MDA8 O<sub>3</sub> from step 1. In this way, the uncertainty of the modelling is further reduced and the final estimation of MDA8 O<sub>3</sub> is achieved. Compared to traditional models, the two-step model is trained not only with Ontario data but also with data in nearby regions, which captures broader regional patterns and long-range transport that influence O<sub>3</sub> in Ontario, especially in border areas.

Specifically, step 1 is formulated as Equation 1:

$$O_{3\_surrounding} = f_1(T, Ps, RH, WS, Fdir, BLH, O_{3EAC4}, OH, NO_2, NO, HCHO, LUT, NDVI, POP) \quad (1)$$

where  $O_{3\_surrounding}$  represents the MDA8 O<sub>3</sub> estimation from stations surrounding Ontario, and  $f_1$  denotes the LightGBM1 model illustrated in Figure 2a. All predictor variables are listed in Table 1. Using the trained  $f_1$ , the MDA8 O<sub>3</sub> is estimated at each station and grid in Ontario, i.e.,  $O_{3,f_1}$ .

Step 2 integrates this initial estimate ( $O_{3,f_1}$ ) to predict the final O<sub>3</sub> in Ontario as Equation 2:

$$O_{3\_ontario} = f_2(O_{3,f_1}, T, Ps, RH, WS, Fdir, BLH, O_{3EAC4}, OH, NO_2, NO, HCHO, LUT, NDVI, POP) \quad (2)$$

where  $O_{3\_ontario}$  represents the MDA8 O<sub>3</sub> measurements from stations surrounding Ontario, and  $f_2$  represents the LightGBM2 (Figure 2a). Except for including  $O_{3,f_1}$ , the remaining variables used in step 2 are the same as (1) and listed in Table 1.

## 2.3 Validation and comparison

To validate the modelling accuracy, different training and validation datasets are selected. For step 1, the surface MDA8 O<sub>3</sub> from the surrounding stations and the data from Ontario stations are used for model training and validation, respectively. For step 2, the data are randomly divided into 10 groups based on the stations, i.e., data samples from the same station will not be split. This way of data split is considered the most reliable for validating spatial extrapolation (Li et al., 2020). Eight groups of data are used for model training, and the rest two groups for validation. Figure 1 shows the stations selected for model training (red points) and validation (star signs) in step 2.

In addition, the estimated MDA8 O<sub>3</sub> by the two-step model is also compared with two published datasets on the global scale, as no gridded MDA8 O<sub>3</sub> datasets specifically for Ontario. These two datasets include the daily MDA8 O<sub>3</sub> data from 2019 to 2021 produced by Wang et al. (2025) and the annual O<sub>3</sub> from 2004 to 2017 produced by Delang et al. (2021). The comparisons of MDA8 O<sub>3</sub> estimations are based on their agreements with all the *in-situ* MDA8 O<sub>3</sub> measurements in Ontario.

## 2.4 Removing meteorological impacts

To quantify the non-meteorological impacts on O<sub>3</sub> trends, primarily those associated with anthropogenic activities,

meteorological-adjusted O<sub>3</sub> trends are derived. Meteorological impacts are removed using a multiple linear regression model, as Equation 3 following previous studies (Tai et al., 2010; Yang et al., 2019):

$$C(t) = \sum_{i=1}^n a_i V_{i(t)} + b + r_{(t)} \quad (3)$$

where  $C(t)$  represents the daily MDA8 O<sub>3</sub> from 2004 to 2023 obtained by two-step model;  $n$  is the number of meteorological variables, including all the inputs for the two-step model (Fdir, T, RH, WS and Ps);  $i$  is an index for the meteorological variables.  $V_{i(t)}$  is the daily meteorological variable  $i$  from 2004 to 2023;  $a_i$  and  $b$  are the regression coefficient for meteorological variable  $i$  and the intercept of regression;  $r_{(t)}$  is the residual term, which represents the MDA8 O<sub>3</sub> after removing the meteorological impact (i.e., met-adjusted MDA8 O<sub>3</sub>).

## 3 Results

### 3.1 Accuracy of the estimated surface O<sub>3</sub> concentrations

Figure 4a shows the validation of the estimated MDA8 O<sub>3</sub> by the two-step model against the *in-situ* measured MDA8 O<sub>3</sub>. By station-based validation, the overall agreement is well, with R<sup>2</sup> of 0.83 and RMSE of 4.99 ppb. For each step in the modelling, the initial estimation of MDA8 O<sub>3</sub> using surrounding stations achieves an accuracy of R<sup>2</sup> being 0.74 and RMSE being 6.05 ppb, and the final estimation further increases the R<sup>2</sup> by 12% and decreases the RMSE by 21%. Compared to traditional modelling (Figure 4b), on average, the two-step modelling increases R<sup>2</sup> by 10% and decreases RMSE by 16%, indicating the advantages of considering surrounding stations and incorporating spatial and temporal dependencies. In addition, the two-step modelling has improved the R and RMSE from the traditional modelling, quantified as [100 × (two-step modelling - traditional modelling)/traditional modelling] for both R<sup>2</sup> and RMSE. Spatially, Figures 4c,d show that R<sup>2</sup> is increased to >15% and RMSE is decreased to <25%. The improvement is the higher in the south than in the north, likely because most of the surrounding stations are located around southern Ontario.

The improved accuracy is especially important for better capturing O<sub>3</sub> concentrations on polluted days. Figure 5 shows the MDA8 O<sub>3</sub> concentrations over southern Ontario on 20 July 2021, when high levels of air pollution were reported due to the wildfire smoke ([https://ottawa.citynews.ca/2021/07/20/special-air-quality-advisory-issued-for-southern-ontario-due-to-wildfire-smoke-3969377/?utm\\_source=chatgpt.com](https://ottawa.citynews.ca/2021/07/20/special-air-quality-advisory-issued-for-southern-ontario-due-to-wildfire-smoke-3969377/?utm_source=chatgpt.com)). Figures 5a,b show the extremely high O<sub>3</sub> concentrations from both models estimated (the base map) and *in-situ* observed (circles) results. However, traditional modelling underestimates the high MDA8 O<sub>3</sub> concentrations over southeastern Ontario, as well as over the coastal area of southwestern Ontario. Figures 5b,c quantify that traditional modelling underestimates the MDA8 O<sub>3</sub> concentrations by a relative difference (RD) of 7%, while the two-step modelling has a good agreement with observation, indicated by an improved RD of 0.3%.

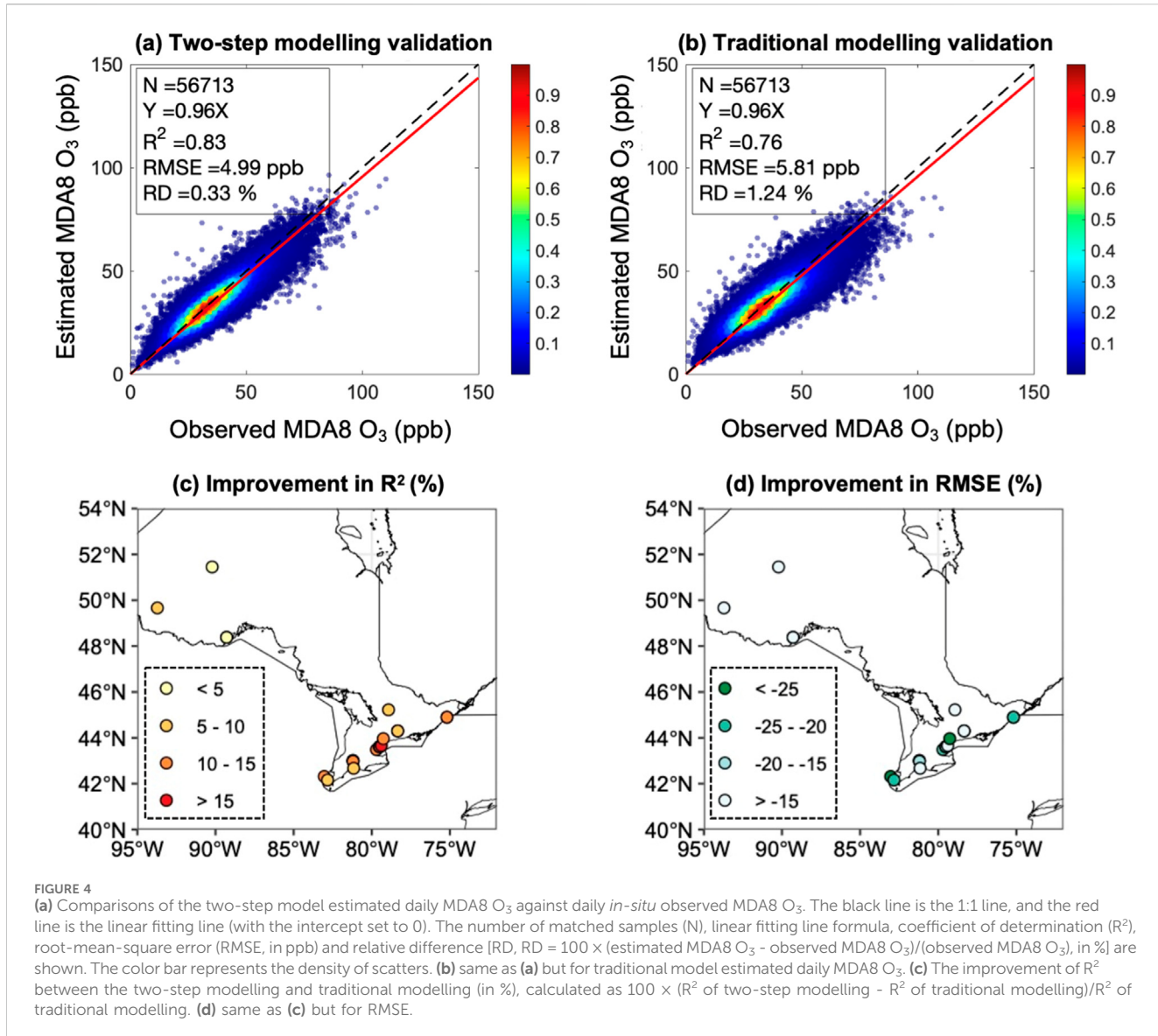


Figure 6 compares the estimated MDA8 O<sub>3</sub> using the two-step model with two published MDA8 O<sub>3</sub> datasets. Note that these two datasets are aimed at offering MDA8 O<sub>3</sub> concentrations globally, rather than specifically for Ontario. All the data from *in-situ* MDA8 O<sub>3</sub> monitoring stations over Ontario are used to compare the accuracy of the three MDA8 O<sub>3</sub> datasets. Compared to the daily MDA8 O<sub>3</sub> dataset over 2019–2021 from Wang et al. (2025) (Figure 6b), the two-step model (Figure 6a) enhances the R<sup>2</sup> by 11% and reduces RMSE by 24% and RD by 58%. In a longer period over 2004–2017, the estimated yearly MDA8 O<sub>3</sub> concentrations (Figure 6c) are compared with those from Delang et al. (2021) (Figure 6d). The two-step model estimated MDA8 O<sub>3</sub> shows a better agreement with the *in-situ* O<sub>3</sub>, with R<sup>2</sup> higher by 0.3 and RMSE lower by 5.5 ppb. Also, a clear overestimation of MDA8 O<sub>3</sub> is apparent in Delang et al. (2021) with RD of 17%, while the RD in our dataset is only about 0.2%.

### 3.2 Spatial variations of surface O<sub>3</sub> concentrations over Ontario

Based on the daily MDA8 O<sub>3</sub> concentrations estimated by the two-step model, the spatial variations of O<sub>3</sub> over Ontario from 2004 to 2023 are studied. Figure 7 shows the 20-year mean daily MDA8 O<sub>3</sub> over Ontario, capturing the high values over southern Ontario. In general, Table 2a shows that the mean concentrations of daily MDA8 O<sub>3</sub> over southern Ontario ( $36.83 \pm 9.82$  ppb) is about 4 ppb higher than over Ontario ( $32.94 \pm 8.21$  ppb). Compared to the north, southern Ontario is more densely populated and urbanized, with the western edge close to the major populated industrial cities such as Detroit and Windsor (Figure 7b). Therefore, the high MDA8 O<sub>3</sub> concentrations over southern Ontario are largely attributed to industrial emissions of O<sub>3</sub> precursors such as nitrogen oxides and sulfur oxides (McGuire et al., 2011; Halla et al., 2011). Owing to the high spatial resolution (10 km) of this dataset, the regional difference is also observed among southern Ontario. In Toronto city, due to the higher

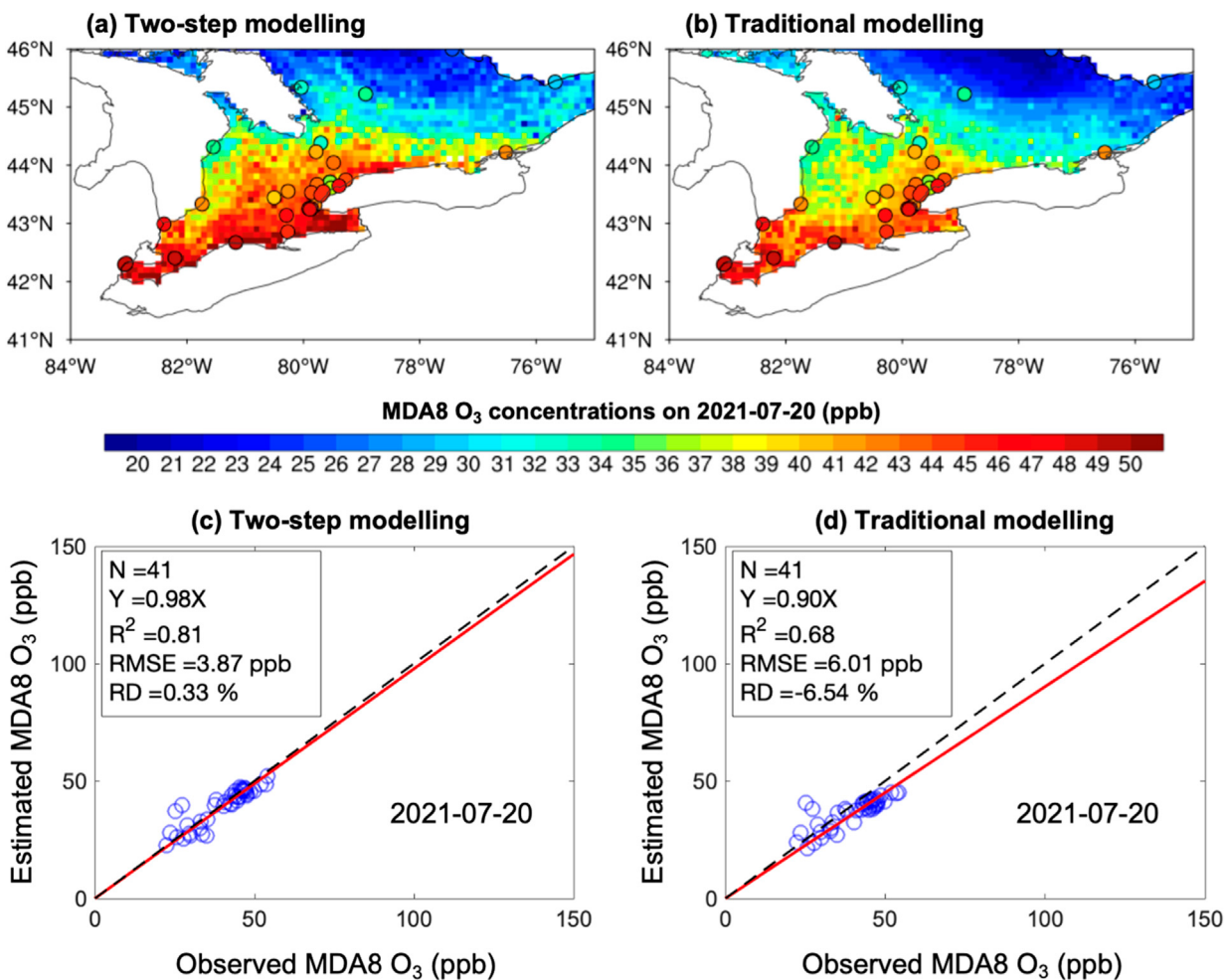


FIGURE 5

(a) The MDA8 O<sub>3</sub> spatial distribution from the two-step modelling estimation (the base map) and *in-situ* observation (the circles) on 20 July 2021. (b) same as (a) but from the traditional modelling estimation. (c) Comparisons of daily MDA8 O<sub>3</sub> between the two-step model estimations and *in-situ* observations on 20 July 2021. The black line is the 1:1 line, and the red line is the linear fitting line (with the intercept set to 0). The number of matched samples (N), linear fitting line formula, coefficient of determination ( $R^2$ ), root-mean-square error (RMSE, in ppb) and relative difference [RD, RD = 100 × (estimated MDA8 O<sub>3</sub> - observed MDA8 O<sub>3</sub>) / (observed MDA8 O<sub>3</sub>), in %] are shown. (d) same as (c) but for traditional model estimation.

rate of ozone depletion by traffic-emitted NO<sub>x</sub> (Geddes et al., 2009; Huryn and Gough, 2014), the O<sub>3</sub> concentrations (30–32 ppb) are lower than the concentrations (>35 ppb) over southwestern Ontario (Figure 7b). In addition, the transported O<sub>3</sub> and precursor by southwesterly airflows from USA contribute to the higher O<sub>3</sub> concentrations over southwestern Ontario than Toronto city as well (Makar et al., 2010; Ministry of the Environment and Climate Change, 2018c). At regions near lakeshore over southern Ontario, Figure 6a shows lower MDA8 O<sub>3</sub> concentrations than inland, indicating the influence of land-lake breeze that dilutes the O<sub>3</sub> concentrations near lake and results in an O<sub>3</sub> gradient at the lake edge (Huang and Donaldson, 2024).

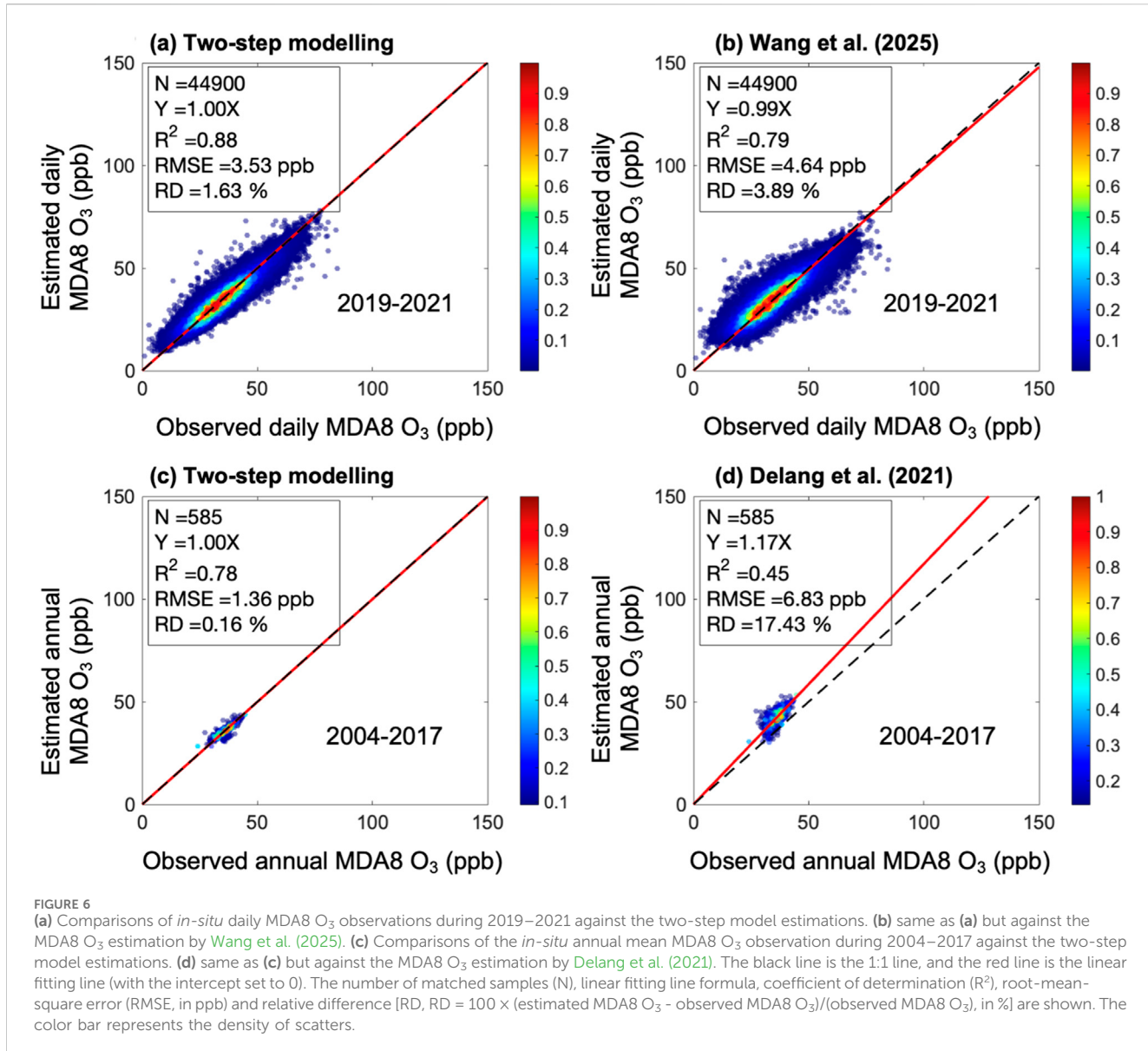
### 3.3 Temporal variations of surface O<sub>3</sub> concentrations over Ontario

#### 3.3.1 Seasonal variation

Seasonality greatly modulates the magnitude of daily MDA8 O<sub>3</sub> concentrations in Ontario (Leung et al., 2021). For both Ontario and

southern Ontario (Table 2a), MDA8 O<sub>3</sub> concentrations during warm seasons (spring and summer) are higher than the ones during cold seasons (autumn and winter), due to the more active photochemical O<sub>3</sub> formation under higher temperature and solar radiation (Crutzen, 1974), as well as the strongest stratospheric intrusions in spring (Monks, 2000). Figures 8a–d show the spatial distributions of MDA8 O<sub>3</sub> over southern Ontario in each season. High MDA8 O<sub>3</sub> concentrations are more homogeneously in spring than in summer when MDA8 O<sub>3</sub> hotspots are concentrated over the western region (Figure 8a vs; Figure 8b), which is also reflected in the overall higher MDA8 O<sub>3</sub> concentrations in spring than in summer (Table 2a). Such spatial inhomogeneity in summer continues in autumn but subsides in winter when MDA8 O<sub>3</sub> concentrations become homogeneously low over entire southern Ontario (Figure 8c vs; Figure 8d).

Figure 8f further shows the 20-year mean MDA8 O<sub>3</sub> in each month over four subregions of southern Ontario: the west, central west, central east and east regions (Figure 8e). Among the four subregions, O<sub>3</sub> concentrations in the west is the highest throughout



the year with a clear peak (47.06 ppb) in June. In contrast, the east shows the lowest MDA8 O<sub>3</sub> concentrations during April–October among all the subregions, with a peak (43.66 ppb) in April. Both central west (45.28 ppb) and central east (45.16 ppb) show a peak in May, with intermediate MDA8 O<sub>3</sub> concentrations between the west and east. The spring O<sub>3</sub> maximum is widely found over the midlatitudes of Northern Hemisphere (Monks, 2000; Gaudel et al., 2018), which are attributed to the enhanced photochemistry in spring after the accumulation of O<sub>3</sub> precursor in winter (Penkett and Brice, 1986), as well as stratospheric intrusions (Monks, 2000). However, in summer, high MDA8 O<sub>3</sub> concentrations still prevail over southwestern Ontario, with much higher values than in the other seasons. The summer O<sub>3</sub> maximum is typical for regions dominated by anthropogenic photochemical ozone production and long-range transport (Singh et al., 1967; Logan, 1985). Due to being closer to industrial regions and being influenced by O<sub>3</sub> transported by southwesterly wind, southwestern

Ontario shows a summer peak in O<sub>3</sub>. The different seasonal peaks between southeastern and southwestern Ontario indicate different sources of O<sub>3</sub> over southern Ontario.

### 3.3.2 Long-term trend

The constructed dataset covers 20 years from 2004 to 2023, enabling investigation of the MDA8 O<sub>3</sub> trend during the 20 years over Ontario, especially over southern Ontario where O<sub>3</sub> pollution is severest in the province. Table 2b summarizes the MDA8 O<sub>3</sub> trends during 2004–2023 for the entire Ontario and southern Ontario, respectively. Over the entire Ontario, a significant ( $p < 0.05$ ) increase of  $0.05 \pm 0.04$  ppb/year is observed. In contrast, southern Ontario exhibits a non-significant ( $p > 0.05$ ) trend of  $-0.01 \pm 0.05$  ppb/year, which agrees with the no clear O<sub>3</sub> trends in the recent 10 years documented the Air Quality in Ontario Report (Ministry of the Environment and Climate Change, 2018a; Ministry of the Environment and Climate

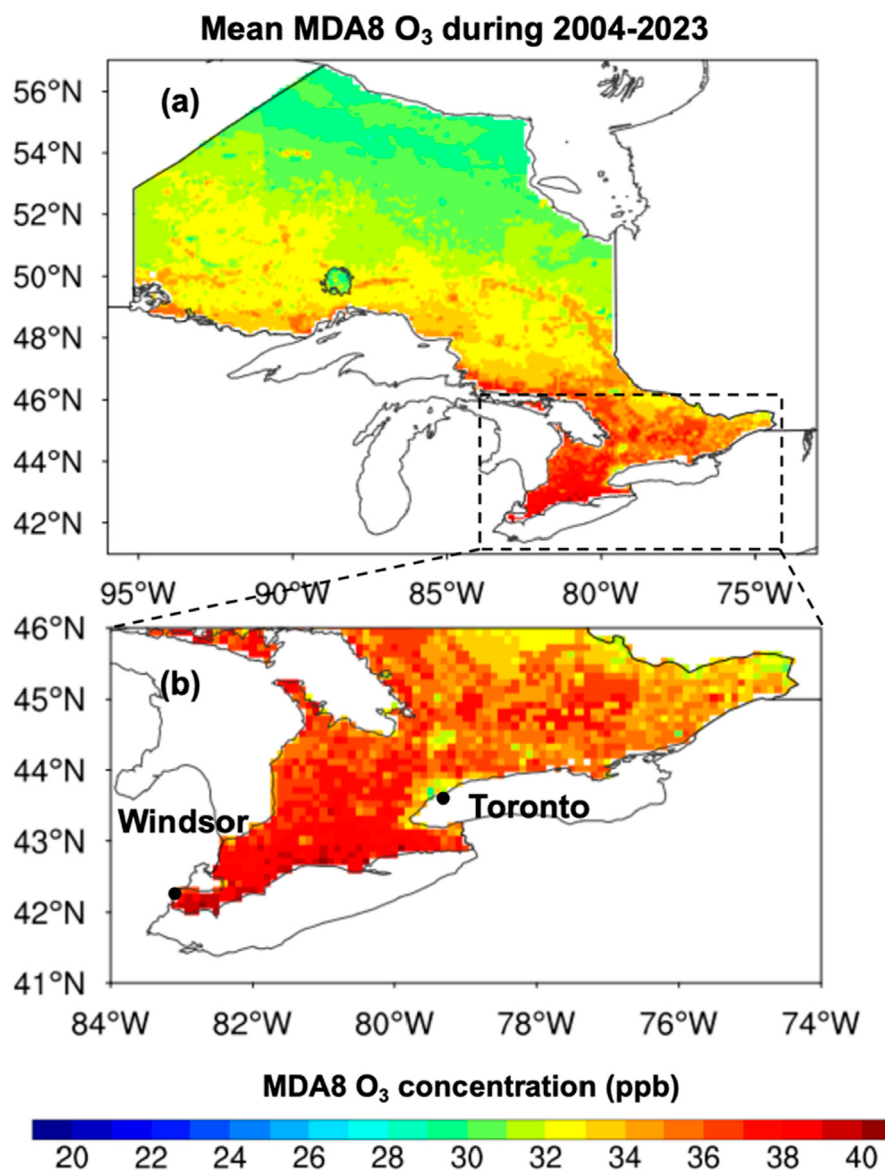


FIGURE 7

(a) The spatial distribution of the mean MDA8 O<sub>3</sub> (in ppb) over Ontario during 2004–2023. (b) Same as (a) but for southern Ontario (up to 46°N). The mean MDA8 O<sub>3</sub> concentrations over Ontario and southern Ontario are shown in Table 2a. The two dots indicate the locations of Toronto and Windsor.

Change, 2018b; Ministry of the Environment and Climate Change, 2018c; Ministry of the Environment and Climate Change, 2019; Ministry of the Environment and Climate Change, 2020; Ministry of the Environment and Climate Change, 2021; Ministry of the Environment and Climate Change, 2022). Because most of the O<sub>3</sub> monitoring stations are located in southern Ontario (Figure 1), the regional discrepancy suggests an increase in MDA8 O<sub>3</sub> in northern Ontario, where monitoring coverage is limited. Despite the overall non-significant trend over southern Ontario, spatial heterogeneity is clear. Figure 9a shows the distributions of the MDA8 O<sub>3</sub> trend for southern Ontario, which reveals a significant ( $p < 0.05$ ) decreasing trend over southwestern Ontario at a rate about  $-0.1$  ppb/year. However, over southeastern Ontario, the

MDA8 O<sub>3</sub> concentrations increase significantly at a rate about  $0.1$  ppb/year.

Given the significant influence of meteorological conditions on long-term MDA8 O<sub>3</sub> trends, the meteorological-impact-removed, namely, met-adjusted, MDA8 O<sub>3</sub> trend (see Section 2.4) during 2004–2023 is further analyzed. Table 2b shows that for the entire Ontario, the magnitude of met-adjusted MDA8 O<sub>3</sub> trend remains the same as the original trend ( $0.05 \pm 0.04$  ppb/year), indicating that the general trend in Ontario is dominated by non-meteorological drivers. For southern Ontario, compared to the original trend, met-adjusted MDA8 O<sub>3</sub> exhibits a slightly stronger decline ( $-0.02$  ppb/year), and a greater magnitude and a broader area of decrease in southwestern Ontario (Figure 9b). This indicates that non-meteorological drivers, primarily emission

TABLE 2 (a) The annual and seasonal mean MDA8 O<sub>3</sub> concentrations  $\pm$  standard deviations averaged over Ontario and southern Ontario during 2004–2023 (in ppb). (b) The annual and seasonal MDA8 O<sub>3</sub> trends  $\pm$ 95% confidence interval for Ontario and southern Ontario during 2004–2023 (in ppb/year)<sup>a</sup>.

(a) MDA8 O <sub>3</sub> concentrations (ppb)			
	Ontario	Southern Ontario (<46°N)	
Annual mean	32.94 $\pm$ 8.21	36.83 $\pm$ 9.82	
Spring (MAM)	40.42 $\pm$ 6.28	43.60 $\pm$ 7.53	
Summer (JJA)	31.69 $\pm$ 9.32	39.63 $\pm$ 11.12	
Autumn (SON)	27.80 $\pm$ 6.33	31.26 $\pm$ 8.39	
Winter (DJF)	31.75 $\pm$ 4.12	32.71 $\pm$ 5.70	

(b) Trends (ppb/year) for original and met-adjusted MDA8 O <sub>3</sub>				
	Ontario		Southern Ontario (<46°N)	
	Original	Met-adjusted	Original	Met-adjusted
Annual mean	0.05 $\pm$ 0.04**	0.05 $\pm$ 0.04**	-0.01 $\pm$ 0.05	-0.02 $\pm$ 0.05
Spring (MAM)	-0.01 $\pm$ 0.14	0.01 $\pm$ 0.14	-0.06 $\pm$ 0.17	-0.06 $\pm$ 0.08
Summer (JJA)	0.08 $\pm$ 0.14	0.04 $\pm$ 0.11	-0.15 $\pm$ 0.17	-0.16 $\pm$ 0.07**
Autumn (SON)	0.11 $\pm$ 0.09**	0.10 $\pm$ 0.09**	0.08 $\pm$ 0.15	0.07 $\pm$ 0.07
Winter (DJF)	0.04 $\pm$ 0.05	0.07 $\pm$ 0.09	0.09 $\pm$ 0.07**	0.07 $\pm$ 0.04**

<sup>a</sup>The annual trend is calculated from the time series of the deseasonalized monthly mean MDA8 O<sub>3</sub>, and the seasonal trend is calculated from the time series of the seasonal mean MDA8 O<sub>3</sub> in each year. Two asterisks indicate the trend is significant with a p-value<0.05. In the table, MAM indicates March-April-May, JJA June-July-August, SON September-October-November, and DJF December-January-February.

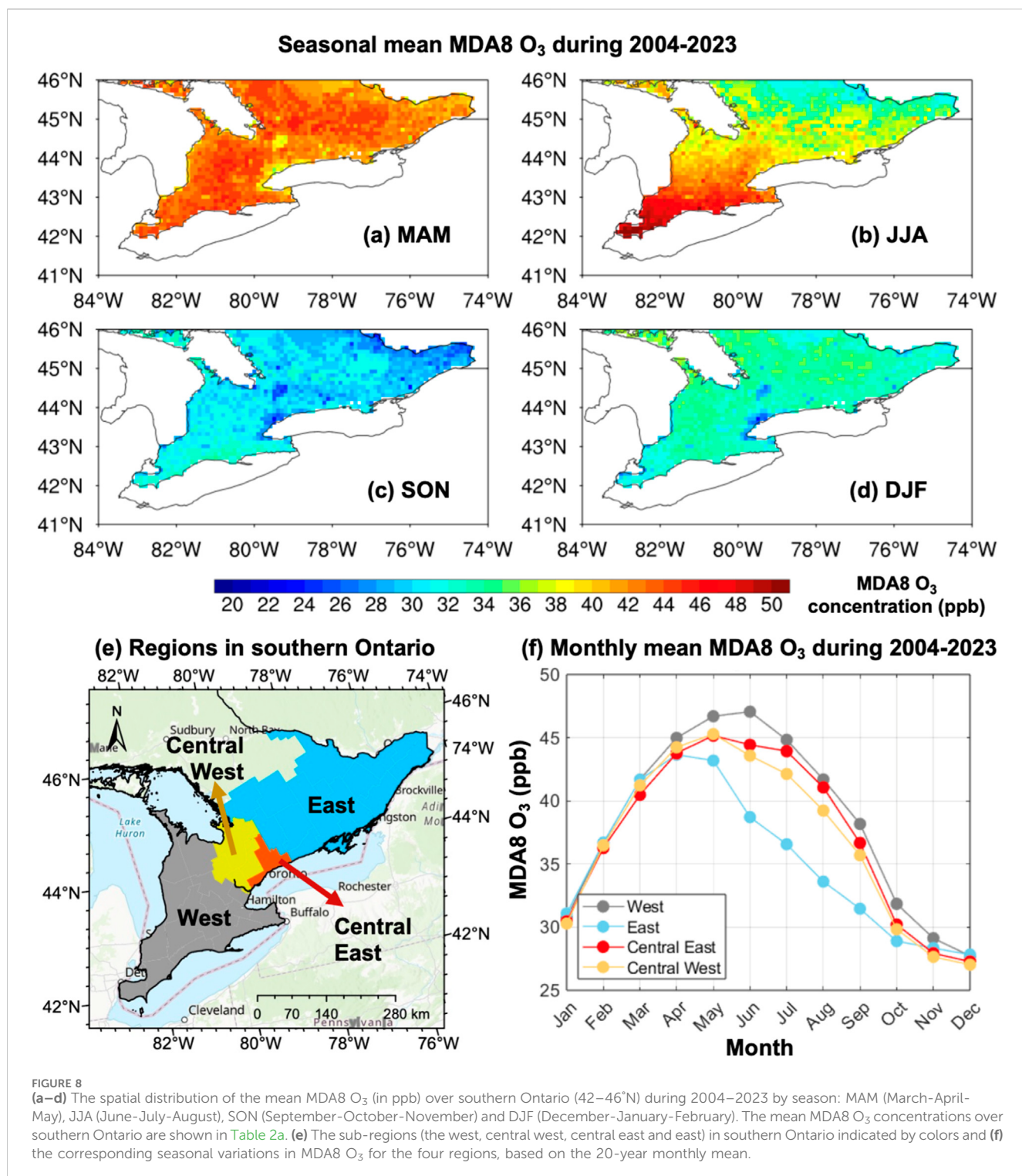
reductions, is greater than what is observed from the real MDA8 O<sub>3</sub> trend and the meteorological impact on MDA8 O<sub>3</sub> trend is positive, which partially offsets the impact of the reduction of precursor emissions.

Seasonally, over 2004–2023, distinct difference also shows in trends over the entire Ontario and southern Ontario. For the entire Ontario, both original and met-adjusted MDA8 O<sub>3</sub> trends show significant increases only in autumn with similar magnitudes (about 0.10  $\pm$  0.09 ppb/year), while trends in other seasons are not statistically significant (Table 2b). For southern Ontario, MDA8 O<sub>3</sub> decreases in warm seasons (spring and summer), especially in summer, which is in contrast to its increases in cold seasons (autumn and winter), especially in winter (Figures 10a,b vs; Figures 10c,d). There are larger areas with significant trends in cold seasons than in the warm seasons, with largest areas with increasing trends in winter across southern Ontario. In comparison, warm seasons show the significant decreasing trends only over southwestern Ontario. Correspondingly, in the sub-regions over southern Ontario (Figure 9b), wintertime MDA8 O<sub>3</sub> increases significantly in all the four sub-regions, while summertime MDA8 O<sub>3</sub> decreases significantly only the west (Table 3). The decrease of MDA8 O<sub>3</sub> in spring and increase of MDA8 O<sub>3</sub> in autumn are both not significant in all the four sub-regions (Table 3).

Similar to the annual mean (Figure 9), after removing the meteorological impact, the met-adjusted MDA8 O<sub>3</sub> trend in warm seasons shows a greater decrease with broader areas, particularly in southeastern Ontario (Figures 10e,f). Particularly, the central west and central east regions show significantly decrease in met-adjusted O<sub>3</sub>

trend in summer, in contrast to the non-significant actual O<sub>3</sub> trends in those regions (Table 3). The significant decrease in summertime O<sub>3</sub> over southern Ontario is mainly due to the progressive controls of NO<sub>x</sub> emissions in Ontario and the USA, which decrease local ozone formation and transboundary influences (Ministry of the Environment and Climate Change, 2018). Despite being offset by meteorological-driven increases in O<sub>3</sub>, the actual trend remains negative, significantly with a magnitude larger than 0.2 ppb/year in southeastern Ontario (Figure 10b). In summer, a comparison of the MDA8 O<sub>3</sub> trend in southern Ontario and with that in the entire Ontario (Table 2b) suggests an increasing O<sub>3</sub> trend in northern Ontario.

During cold seasons, MDA8 O<sub>3</sub> increases non-significantly in autumn, but significantly in winter over southern Ontario, especially in southeastern Ontario (Figures 10d,h, Table 2b). The wintertime MDA8 O<sub>3</sub> trends in the four sub-regions of southeastern Ontario all turn from significant increase to non-significant after removing meteorological impacts (Table 3). The increased O<sub>3</sub> during cold seasons is likely to mainly attribute to an increase in the global background O<sub>3</sub> concentrations (Reid et al., 2008; Parrish et al., 2012), which is positively overlaid by the impact of meteorological variability over 2004–2023. In contrast to the non-significant MDA8 O<sub>3</sub> trends in autumn over southern Ontario, the significant increase over the entire Ontario in autumn implies a pronounced increase over northern Ontario (Table 2b). The increasing MDA8 O<sub>3</sub> over northern Ontario during summer and autumn could be driven by wildfire emissions, as it coincides with the wildfire season as well as the increasing wildfire activities, e.g., area burned and number of large fires in Ontario (Hanes et al., 2019; Jain et al., 2024).



### 3.4 O<sub>3</sub> exceedance days

The 2021 WHO air quality guidelines recommend that the health level of MDA8 O<sub>3</sub> concentrations should be lower than a threshold of 100 µg/m<sup>3</sup> or 50 ppb. Thus, a day with MDA8 O<sub>3</sub> concentrations larger than this threshold is referred as the O<sub>3</sub> exceedance day. Based on the constructed daily O<sub>3</sub> dataset, Figure 11a shows the mean exceedance days per year during

2004–2023 at each of the 10-km grids. The number of exceedance days is largest around the most southwestern region, reaching ~80 days per year. The number decreases gradually northward, with ~10 days per year in the northern region. Such a spatial pattern resembles O<sub>3</sub> concentrations (Figure 7b), indicating concurrent higher O<sub>3</sub> concentrations and more O<sub>3</sub> exceedance days.

Figure 11b shows a significant decreasing trend in the number of O<sub>3</sub> exceedance days, particularly in southwestern Ontario by up to

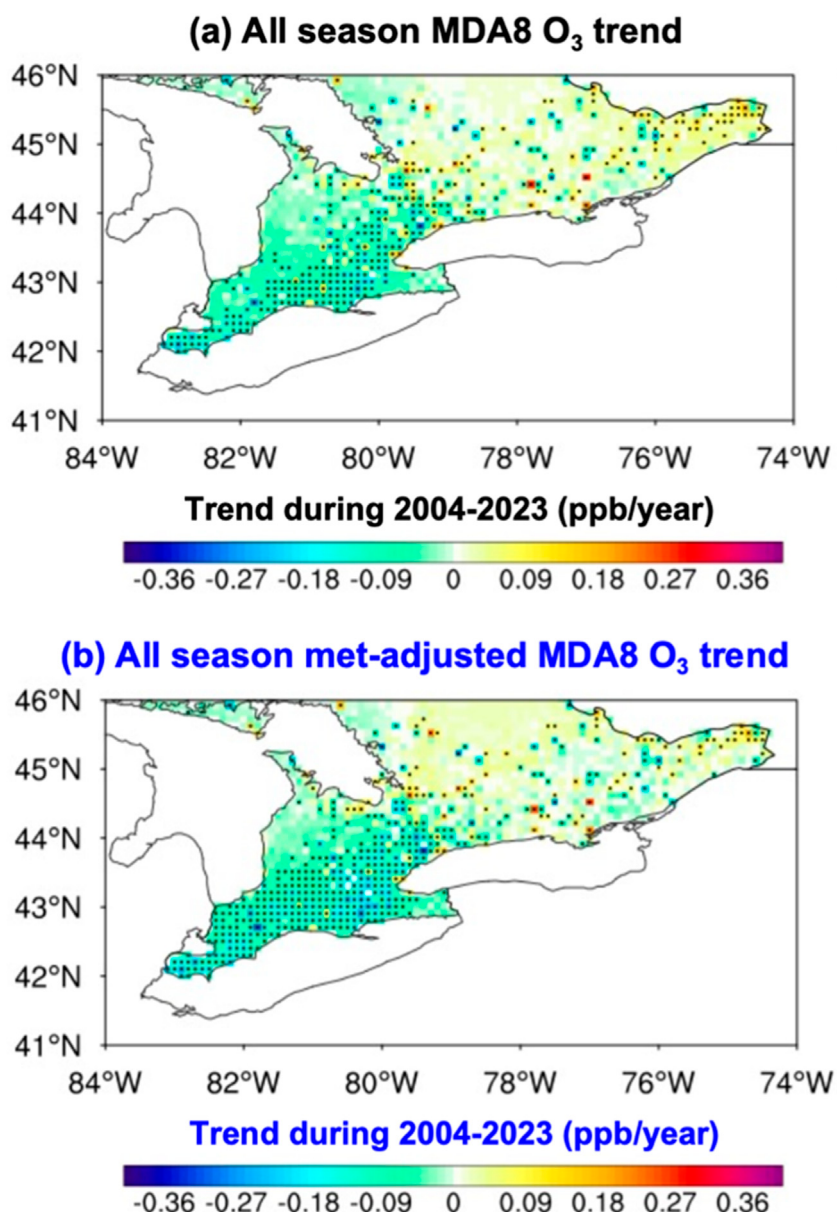


FIGURE 9

(a) The spatial distribution of MDAB O<sub>3</sub> trend over southern Ontario during 2004–2023 (in ppb/year). Note that the trend is calculated from the time series of the deseasonalized monthly mean MDAB O<sub>3</sub>. Dotted area indicates trends are significant at the 95% level. (b) same as (a) but for the spatial distribution of met-adjusted trend.

4 days/year (equivalent to about 15%/year). Differently from the slight increasing trend in O<sub>3</sub> concentrations over southeastern Ontario (Figure 9a), the frequency of high O<sub>3</sub> concentrations is decreasing over the entire southern Ontario. This improvement shows the effective controls of O<sub>3</sub> pollution in Ontario.

## 4 Discussion and conclusion

To study the long-term and spatially explicit O<sub>3</sub> concentrations and trends over Ontario, we constructed a dataset of daily MDA8 O<sub>3</sub> concentrations with a spatial resolution of 10 km for Ontario. This dataset is constructed based on surface O<sub>3</sub> observations at individual

stations from NAPS program and USA EPA (Table 1), using a two-step statistical model built by LightGBM algorithm. The two-step model integrates MDA8 O<sub>3</sub> measurements from neighboring stations within 500 km, along with data from adjacent grid points (8 surrounding grids) and time windows ( $\pm 1$  day), to improve modelling accuracy. Multi-sources input data, including meteorological, satellite and emission data, are used as the predictors (Table 1).

The modelling performance is validated using station-based data to represent spatial predictability. Across validation stations, the two-step model achieves high accuracy, with an R<sup>2</sup> of 0.82 and a RMSE of 4.99 ppb (Figure 4). Our results are compared with two global MDA8 O<sub>3</sub> datasets from Wang et al. (2025) at daily time step

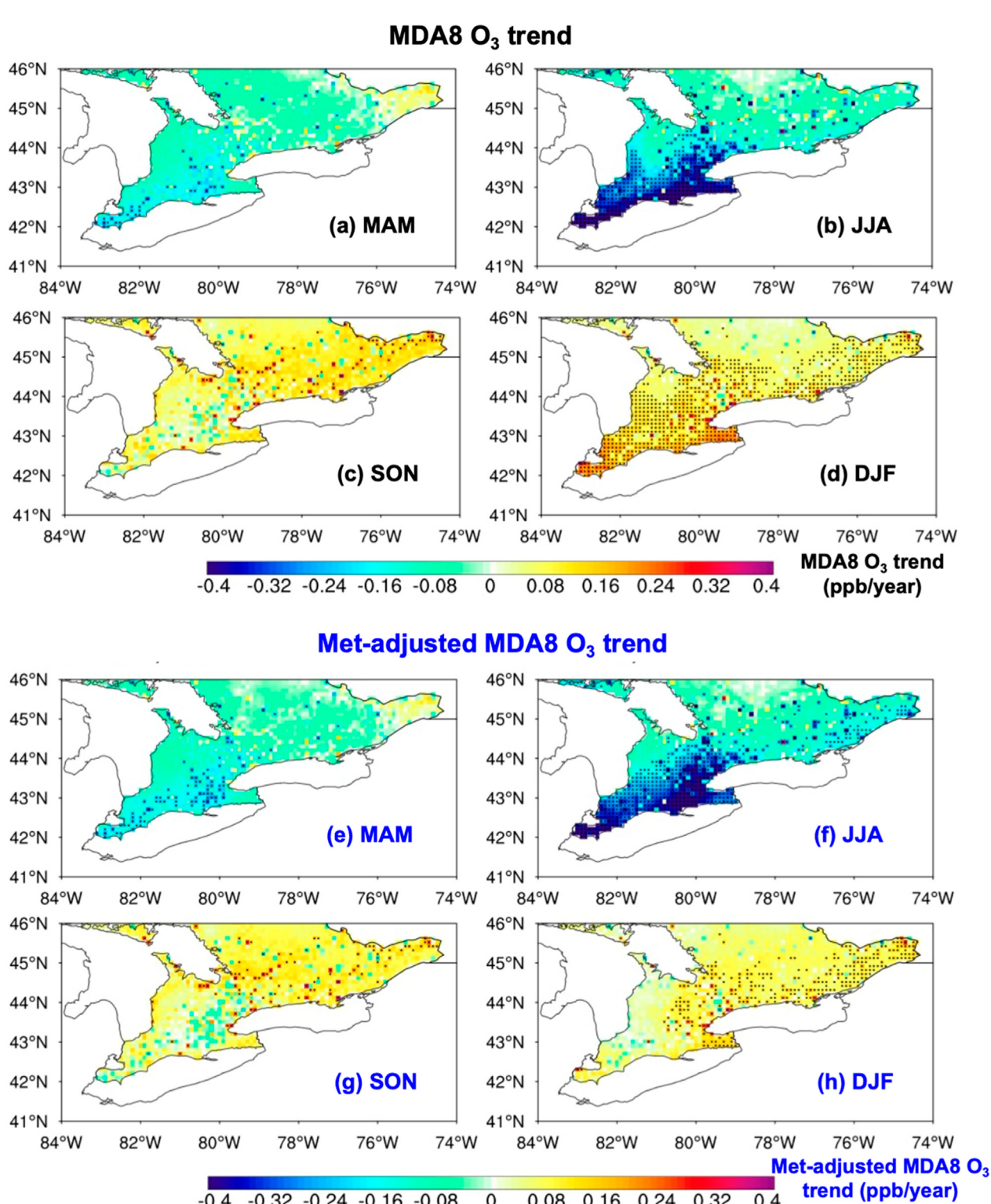


FIGURE 10

(a–d) The spatial distribution of MDA8 O<sub>3</sub> trend over southern Ontario in each season during 2004–2023 (in ppb/year). Note that the trend is calculated from the time series of the seasonal mean MDA8 O<sub>3</sub> in each year. Dotted area indicates the trends being significant at the 95% level. The mean trend  $\pm$ 95% confidence interval during 2004–2023 is given in Table 2b, calculated by the seasonal mean MDA8 O<sub>3</sub> time series averaged over southern Ontario. (e–h) same as (a–d) but for met-adjusted trend.

TABLE 3 The MDA8 O<sub>3</sub> trends  $\pm$ 95% confidence interval by season for the four regions (see Figure 8c) in southern Ontario during 2004–2023 (in ppb/year)<sup>a</sup>.

Season	Region	Trend (ppb/year)	Met-adjusted trend (ppb/year)
Spring (MAM)	West	-0.09 $\pm$ 0.16	0.01 $\pm$ 0.14
	East	-0.03 $\pm$ 0.14	0.01 $\pm$ 0.14
	Central West	-0.04 $\pm$ 0.16	0.03 $\pm$ 0.15
	Central East	0.01 $\pm$ 0.16	0.06 $\pm$ 0.16
Summer (JJA)	West	-0.23 $\pm$ 0.15**	-0.26 $\pm$ 0.21**
	East	-0.07 $\pm$ 0.14	-0.13 $\pm$ 0.16
	Central West	-0.15 $\pm$ 0.15	-0.20 $\pm$ 0.17**
	Central East	-0.15 $\pm$ 0.21	-0.21 $\pm$ 0.17**
Autumn (SON)	West	0.12 $\pm$ 0.15	0.10 $\pm$ 0.16
	East	0.14 $\pm$ 0.13	0.11 $\pm$ 0.16
	Central West	0.14 $\pm$ 0.15	0.11 $\pm$ 0.17
	Central East	0.16 $\pm$ 0.15	0.17 $\pm$ 0.17
Winter (DJF)	West	0.16 $\pm$ 0.08**	0.12 $\pm$ 0.18
	East	0.09 $\pm$ 0.06**	0.12 $\pm$ 0.11
	Central West	0.14 $\pm$ 0.07**	0.11 $\pm$ 0.14
	Central East	0.15 $\pm$ 0.07**	0.15 $\pm$ 0.16

<sup>a</sup>Both the actual O<sub>3</sub> trends and the trend after removing meteorological impact (met-adjusted) are shown. Two asterisks indicate the trend is significant with a p-value < 0.05.

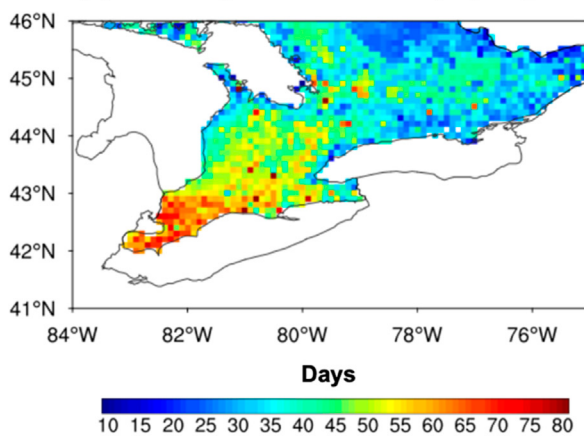
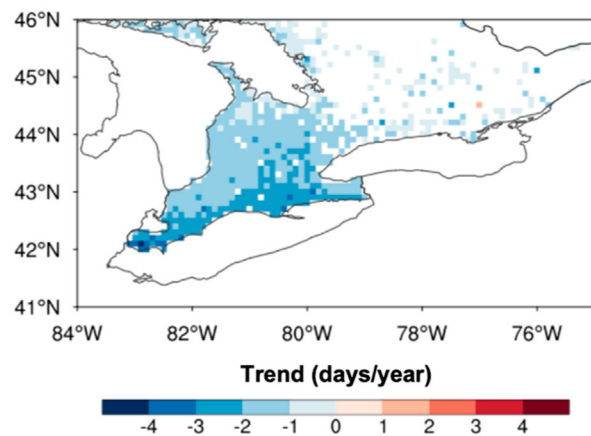
(a) Mean O<sub>3</sub> exceedance days per year(b) Trend in O<sub>3</sub> exceedance days per year

FIGURE 11

(a) The spatial distribution of the mean O<sub>3</sub> exceedance days per year over southern Ontario during 2004–2023. (b) The trend in O<sub>3</sub> exceedance days per year over southern Ontario during 2004–2023 (in days/year). Note that only the grids with trends that are significant at the 95% level are shown.

(2019–2021) and from Delang et al. (2021) at annual time step (2004–2017) (Figure 6). Our dataset shows a better agreement with *in-situ* measurements than both MDA8 O<sub>3</sub> datasets. To test the hypothesis suggested in Introduction, the two-step model is also compared with the traditional model that uses O<sub>3</sub> measurements from stations in Ontario only (Figure 3b). The two-step model improves R<sup>2</sup> by 10% and reduces RMSE by 16% (Figures 4a,b), with greater improvements in southern Ontario (Figures 4c,d) because of inclusion of O<sub>3</sub> data from the high density of surrounding stations.

The two-step model also better captures MDA8 O<sub>3</sub> distributions than the traditional model under heavy pollution conditions (Figure 5).

Based on this long-term and high spatiotemporal-resolution MDA8 O<sub>3</sub> dataset, the spatiotemporal variations of MDA8 O<sub>3</sub> over Ontario are further studied. The spatial distribution captures the higher MDA8 O<sub>3</sub> concentrations over densely populated and urbanized southern Ontario, particularly the southwestern areas that are mostly industrialized and also influenced by the

southwesterly transported air pollutants (Figure 7). The seasonal variations reveal the elevated O<sub>3</sub> concentrations during warm seasons compared to cold seasons (Figures 8a–d; Table 2a). Due to the accumulation of O<sub>3</sub> precursors during winter and frequent stratospheric intrusions, southern Ontario exhibits the highest ozone concentrations in spring. During summer, high O<sub>3</sub> levels persist over southwestern Ontario (Figures 8e,f), with peak values in June (Figure 8f), showing largest spatial heterogeneity among all seasons. This summertime O<sub>3</sub> maximum is typical for regions influenced by intense anthropogenic photochemical ozone production and long-range transport (Singh et al., 1967; Logan, 1985). Southwestern Ontario is greatly impacted by both local and transboundary anthropogenic emissions, including those from the industrialized “Chemical Valley” region and its surroundings (MacDonald and Rang, 2007). The ozone precursors such as VOCs in southwestern Ontario (e.g., Hamilton downtown) can reach 39 µg/m<sup>3</sup> but only 36 µg/m<sup>3</sup> in Toronto (Bari and Kindzierski, 2018). In addition, transport from southwestern Michigan contributes substantially to ozone levels in this region (AQA, 2023).

During 2004–2023, MDA8 O<sub>3</sub> trends show a distinct difference over entire Ontario and southern Ontario. For southern Ontario, there is a non-significant ( $p > 0.05$ ) decrease of 0.01 ppb/year (Table 2b), consistent with the report by Air Quality in Ontario (Ministry of the Environment and Climate Change, 2016–2022). However, the spatial distribution of MDA8 O<sub>3</sub> trends is heterogeneous, revealing a significant decrease in southwestern Ontario (~0.1 ppb/year) and an increase in southeastern Ontario (~0.1 ppb/year) during 2004–2023 (Figure 9a). After removing the meteorological impact, the O<sub>3</sub> trend over southern Ontario shifts to a stronger decrease of -0.02 ppb/year (Table 2b, Figure 9c), suggesting that a meteorological-driven increase in O<sub>3</sub> has partially offset by a decrease in O<sub>3</sub> due to precursor emission reductions. For entire Ontario, both original and met-adjusted MDA8 O<sub>3</sub> increases significantly at a rate about 0.05 ppb/year (Table 2b), indicating that the general trend in Ontario is dominated by non-meteorological drivers.

By season, a significant increase trend occurs during winter across southern Ontario (Figure 10d), likely due to the increase in global background O<sub>3</sub> to some degree (Reid et al., 2008; Parrish et al., 2012). Previous studies have reported increases in the continental or hemispheric background O<sub>3</sub> from measurements at remote stations or through meteorological adjustments (Vingarzan, 2004; Oltmans et al., 2006; Chan, 2009; Chan and Vet, 2010). After removing meteorological influences, the wintertime O<sub>3</sub> trend from 2004 to 2023 becomes statistically non-significant over southern Ontario (Figure 10h; Table 2). This suggests that the positive O<sub>3</sub> trend in winter is largely meteorological-driven. In contrast, O<sub>3</sub> in summer decreases significantly, particularly over southwestern Ontario (Figure 10b). The meteorological-impact-remove trends in summer are more negative in a larger area than the actual trends (Figure 10f; Table 2b), which can be largely attributed to the effectiveness of controlling of precursor emissions (Ministry of the Environment and Climate Change, 2018a). Since its implementation in 1991, the Canada-U.S. Air Quality Agreement (Ozone Annex) has controlled and reduced emissions of NOx and VOCs, which are key precursors to

ground-level O<sub>3</sub>, resulting in clear decreases in O<sub>3</sub> during 2000–2020 (AQA, 2023). These results underscore the long-term benefits of emission control in mitigating summertime ozone pollution across southern Ontario. For the entire Ontario, particularly northern Ontario, MDA8 O<sub>3</sub> increase significantly during autumn (Table 2b), coinciding with the wildfire season and trends (Hanes et al., 2019; Jain et al., 2024). This suggests that wildfire activities could be an important driver for MDA8 O<sub>3</sub> trends in Ontario.

The O<sub>3</sub> exceedance days under the 2021 WHO air quality guidelines are also assessed to reveal the frequency of high O<sub>3</sub> days (Figure 11). Southwestern Ontario experiences more frequent exceedances (50–90 days) than southeastern Ontario (10–50 days). However, the days of exceedances decreases significantly during 2004–2023, particularly in southwestern Ontario (up to 4 days/year, equivalent to 15%/year). This clear reduction highlights a decline in short-term O<sub>3</sub> exposure across southern Ontario owing to the air pollution control.

While the two-step model benefits from incorporating both NAPS and EPA monitoring stations, the two datasets are not strictly harmonized prior to integration. Both networks rely on UV-based ozone measurements and have been jointly used in previous evaluations of the Canada-U.S. Air Quality Agreement (AQA, 2023), suggesting a reasonable degree of consistency of the two datasets. However, this represents a limitation of the current study. For broader-scale applications, particularly those involving transboundary ozone pollution or regulatory and health exposure assessments, it would be advantageous to adopt harmonized *in-situ* observations, such as those provided by the Tropospheric Ozone Assessment Report (TOAR) database (Schultz et al., 2017), to ensure greater consistency and comparability across regions.

In summary, the constructed long-term and high-resolution MDA8 O<sub>3</sub> dataset enables a comprehensive analysis of the spatiotemporal variations of O<sub>3</sub> concentrations and frequencies over the past two decades in Ontario, which cannot be fully resolved from measurements at individual monitoring stations. The two-step model can serve as a novel approach for air pollution mapping on regional scale, overcoming the limitations posed by sparse and unevenly distributed monitoring stations. In future, this validated two-decade MDA8 O<sub>3</sub> dataset is expected to be a reliable data for assessing human and crop exposures in environmental health and agricultural research. For example, it can be aligned with high-resolution data of population, hospital admission, or mortality to quantify health burdens, or combined with high-resolution data of crop maps and phenology to assess cumulative O<sub>3</sub> exposure and potential yield loss. These applications highlight the broader value of this O<sub>3</sub> dataset not only for understanding ozone variability, but for supporting data-based decision-making in public health, environmental management, and food security.

## Data availability statement

Publicly available datasets were analyzed in this study. This data can be found here: The *in-situ* measurement of surface O<sub>3</sub> can be obtained from NAPS (<https://data-donnees.az.ec.gc.ca/>

[data/air/monitor/national-air-pollution-surveillance-naps-program/](https://data.air/monitor/national-air-pollution-surveillance-naps-program/) Data-Donnees/) and EPA ([https://aqs.epa.gov/aqsweb/airdata/download\\_files.html](https://aqs.epa.gov/aqsweb/airdata/download_files.html)). The reanalysis data can be accessed from ERA5 (<https://climate.copernicus.eu/climate-reanalysis>), MERRA-2 (<https://disc.gsfc.nasa.gov/>) and EAC4 (<https://ads.atmosphere.copernicus.eu/datasets/cams-global-reanalysis-eac4>). The MODIS land use and NDVI are from <https://modis.gsfc.nasa.gov/data/>. The population density data can be obtained from GPWv4 (<https://www.earthdata.nasa.gov/data/projects/gpw>). The Ontario MDA8 O<sub>3</sub> dataset from this study can be accessed from <https://geisee-dlsph-utoronto.ca/>.

## Author contributions

ZZ: Formal Analysis, Conceptualization, Writing – original draft, Software, Visualization, Data curation, Methodology, Validation, Investigation. JL: Writing – review and editing, Conceptualization, Funding acquisition, Supervision. EG: Funding acquisition, Writing – review and editing, Conceptualization. YZ: Data curation, Writing – review and editing, Formal Analysis.

## Funding

The author(s) declare that financial support was received for the research and/or publication of this article. This research has been supported by Canadian Institutes of Health Research (CIHR, grant no. PJT186225) and by the Natural Science and Engineering Council of Canada (NSERC, grant no. RGPIN 2020-05136).

## References

- Agudelo-Castaneda, D. M., Calessa Teixeira, E., and Norte Pereira, F. (2014). Time-series analysis of surface ozone and nitrogen oxides concentrations in an urban area at Brazil. *Atmos. Pollut. Res.* 5, 411–420. doi:10.5094/apr.2014.048
- AQA: Review and Assessment of the Canada-U.S. Air Quality Agreement (AQA) (2023). *Report, environment Canada and*. Ottawa and Washington, D.C.: U.S. Environmental Protection Agency. Available online at: <https://www.epa.gov/system/files/documents/2024-03/review-and-assessment-of-the-canada-us-aqa-508-compliance.pdf>.
- Bai, K., Chang, N.-B., Yu, H., and Gao, W. (2016). Statistical bias correction for creating coherent total ozone record from OMI and OMPS observations. *Remote Sens. Environ.* 182, 150–168. doi:10.1016/j.rse.2016.05.007
- Bari, M., and Kindzierski, W. (2018). Ambient volatile organic compounds (VOCs) in Calgary, Alberta: sources and screening health risk assessment. *Sci. Total Environ.* 631–632, 627–640. doi:10.1016/j.scitotenv.2018.03.023
- Bhartia, P. K. (2002). OMI algorithm theoretical basis document volume II, OMI ozone.
- Brook, J. R., Lillyman, C. D., Shepherd, M. F., and Mamedov, A. (2002). Regional transport and urban contributions to fine particle concentrations in southeastern Canada. *J. Air and Waste Manag. Assoc.* 52, 855–866. doi:10.1080/10473289.2002.10470821
- Center For International Earth Science Information Network-CIESIN-Columbia University (2017). Gridded population of the World, version 4 (GPWv4): population density, revision 11 (version 4.11). *Palisades, N. Y Socioecon. Data Appl. Cent. (SEDAC)*. doi:10.7927/H49C6VHW
- Chan, E. (2009). Regional ground-level ozone trends in the context of meteorological influences across Canada and the eastern United States from 1997 to 2006. *J. Geophys. Res. Atmos.* 114. doi:10.1029/2008jd010090
- Chan, E., and Vet, R. (2010). Baseline levels and trends of ground level ozone in Canada and the United States. *Atmos. Chem. Phys.* 10, 8629–8647. doi:10.5194/acp-10-8629-2010
- Chen, B., Wang, Y., Huang, J., Zhao, L., Chen, R., Song, Z., et al. (2023). Estimation of near-surface ozone concentration and analysis of main weather situation in China based on machine learning model and Himawari-8 TOAR data. *Sci. Total Environ.* 864, 160928. doi:10.1016/j.scitotenv.2022.160928
- Crutzen, P. J. (1974). Photochemical reactions initiated by and influencing ozone in unpolluted tropospheric air. *Tellus* 26, 47–57. doi:10.1111/j.2153-3490.1974.tb01951.x
- DeLang, M. N., Becker, J. S., Chang, K.-L., Serre, M. L., Cooper, O. R., Schultz, M. G., et al. (2021). Mapping yearly fine resolution global surface ozone through the Bayesian maximum entropy data fusion of observations and model output for 1990–2017. *Environ. Sci. and Technol.* 55, 4389–4398. doi:10.1021/acs.est.0c07742
- Didan, K. (2021). MODIS/Terra vegetation indices 16-day L3 global 0.05Deg CMG V061. *NASA EOSDIS Land Process. Distrib. Act. Arch. Cent.* doi:10.5067/MODIS/MOD13C1.061
- Fleming, Z. L., Doherty, R. M., Von Schneidemesser, E., Malley, C. S., Cooper, O. R., Pinto, J. P., et al. (2018). Tropospheric Ozone Assessment Report: present-day ozone distribution and trends relevant to human health. *Elem. Sci. Anthropocene* 6 (12). doi:10.1525/elementa.273
- Friedl, M., and Sulla-Menashe, D. (2022). MODIS/Terra+Aqua land cover type yearly L3 global 0.05Deg CMG V061 NASA EOSDIS land processes distributed active archive center. doi:10.5067/MODIS/MCD12C1.061
- Gaudel, A., Cooper, O. R., Ancellet, G., Barret, B., Boynard, A., Burrows, J. P., et al. (2018). Tropospheric Ozone Assessment Report: present-day distribution and trends of tropospheric ozone relevant to climate and global atmospheric chemistry model evaluation. *Elem. Sci. Anthropocene* 6 (39). doi:10.1525/elementa.291
- Geddes, J. A., Murphy, J. G., and Wang, D. K. (2009). Long term changes in nitrogen oxides and volatile organic compounds in Toronto and the challenges facing local ozone control. *Atmos. Environ.* 43, 3407–3415. doi:10.1016/j.atmosenv.2009.03.053
- Halla, J., Wagner, T., Beirle, S., Brook, J., Hayden, K., O'brien, J., et al. (2011). Determination of tropospheric vertical columns of NO<sub>2</sub> and aerosol optical properties

## Acknowledgments

We thank Canada NAPS and USA EPA for providing *in-situ* measurement of surface O<sub>3</sub>. We also thank ERA5, MERRA-2 and EAC4 for the reanalysis data. We acknowledge MODIS for the land use and NDVI data, and GPWv4 for the population density data.

## Conflict of interest

The authors declare that the research was conducted in the absence of any commercial or financial relationships that could be construed as a potential conflict of interest.

The authors declared that one of them is an editorial board member of Frontiers, at the time of submission. This had no impact on the peer review process and the final decision.

## Generative AI statement

The author(s) declare that no Generative AI was used in the creation of this manuscript.

## Publisher's note

All claims expressed in this article are solely those of the authors and do not necessarily represent those of their affiliated organizations, or those of the publisher, the editors and the reviewers. Any product that may be evaluated in this article, or claim that may be made by its manufacturer, is not guaranteed or endorsed by the publisher.

- in a rural setting using MAX-DOAS. *Atmos. Chem. Phys.* 11, 12475–12498. doi:10.5194/acp-11-12475-2011
- Hanes, C. C., Wang, X., Jain, P., Parisien, M.-A., Little, J. M., and Flannigan, M. D. (2019). Fire-regime changes in Canada over the last half century. *Can. J. For. Res.* 49, 256–269. doi:10.1139/cjfr-2018-0293
- Hersbach, H., Bell, B., Berrisford, P., Hirahara, S., Horányi, A., Muñoz-Sabater, J., et al. (2020). The ERA5 global reanalysis. *Q. J. R. meteorological Soc.* 146, 1999–2049. doi:10.1002/qj.3803
- Huang, Y. Y., and Donaldson, D. J. (2024). Measurement report: observations of ground-level ozone concentration gradients perpendicular to the Lake Ontario shoreline. *Atmos. Chem. Phys.* 24, 2387–2398. doi:10.5194/acp-24-2387-2024
- Huryn, S. M., and Gough, W. A. (2014). Impact of urbanization on the ozone weekday/weekend effect in Southern Ontario, Canada. *Urban Clim.* 8, 11–20. doi:10.1016/j.ulim.2014.03.005
- Inness, A., Ades, M., Agustí-Panareda, A., Barré, J., Benedictow, A., Blechschmidt, A.-M., et al. (2019). The CAMS reanalysis of atmospheric composition. *Atmos. Chem. Phys.* 19, 3515–3556. doi:10.5194/acp-19-3515-2019
- Jain, P., Barber, Q. E., Taylor, S. W., Whitman, E., Castellanos Acuna, D., Boulanger, Y., et al. (2024). Drivers and impacts of the record-breaking 2023 wildfire season in Canada. *Nat. Commun.* 15, 6764. doi:10.1038/s41467-024-51154-7
- Johnson, D., Mignacca, D., Herod, D., Jutzi, D., and Miller, H. (2007). Characterization and identification of trends in average ambient ozone and fine particulate matter levels through trajectory cluster analysis in eastern Canada. *J. Air and Waste Manag. Assoc.* 57, 907–918. doi:10.3155/1047-3289.57.8.907
- Khiem, M., Ooka, R., Huang, H., Hayami, H., Yoshikado, H., and Kawamoto, Y. (2010). Analysis of the relationship between changes in meteorological conditions and the variation in summer ozone levels over the Central Kanto area. *Adv. Meteorology* 2010, 349248. doi:10.1155/2010/349248
- Lee, H., Liu, Y., Coull, B., Schwartz, J., and Koutrakis, P. (2011). A novel calibration approach of MODIS AOD data to predict PM 2.5 concentrations. *Atmos. Chem. Phys.* 11, 7991–8002. doi:10.5194/acp-11-7991-2011
- Leung, K. H., Arnillas, C. A., Cheng, V. Y., Gough, W. A., and Arhonditsis, G. B. (2021). Seasonality patterns and distinctive signature of latitude and population on ozone concentrations in Southern Ontario, Canada. *Atmos. Environ.* 246, 118077. doi:10.1016/j.atmosenv.2020.118077
- Li, T., Shen, H., Yuan, Q., and Zhang, L. (2022). A locally weighted neural network constrained by global training for remote sensing estimation of PM<sub>2.5</sub>. *IEEE Trans. Geoscience Remote Sens.* 60, 1–13. doi:10.1109/tgrs.2021.3074569
- Li, T., Shen, H., Zeng, C., and Yuan, Q. (2020). A validation approach considering the uneven distribution of ground stations for satellite-based PM 2.5 estimation. *IEEE J. Sel. Top. Appl. Earth Observations Remote Sens.* 13, 1312–1321. doi:10.1109/jstars.2020.2977668
- Liu, G., Tarasick, D. W., Fioletov, V. E., Sioris, C. E., and Rochon, Y. J. (2009). Ozone correlation lengths and measurement uncertainties from analysis of historical ozonesonde data in North America and Europe. *J. Geophys. Res. Atmos.* 114. doi:10.1029/2008jd010576
- Liu, J., and Cui, S. (2014). Meteorological influences on seasonal variation of fine particulate matter in cities over Southern Ontario, Canada. *Adv. Meteorology* 2014, 1–15. doi:10.1155/2014/169476
- Liu, R., Ma, Z., Gasparri, A., de la Cruz, A., Bi, J., and Chen, K. (2023). Integrating augmented *in situ* measurements and a spatiotemporal machine learning model to back-extrapolate historical particulate matter pollution over the United Kingdom: 1980–2019. *Environ. Sci. and Technol.* 57, 21605–21615. doi:10.1021/acs.est.3c05424
- Liu, X., Bhartia, P., Chance, K., Spurr, R., and Kurosu, T. (2010). Ozone profile retrievals from the ozone monitoring instrument. *Atmos. Chem. Phys.* 10, 2521–2537. doi:10.5194/acp-10-2521-2010
- Liu, X., Zhu, Y., Xue, L., Desai, A. R., and Wang, H. (2022). Cluster-enhanced ensemble learning for mapping global monthly surface ozone from 2003 to 2019. *Geophys. Res. Lett.* 49, e2022GL097947. doi:10.1029/2022gl097947
- Logan, J. A. (1985). Tropospheric ozone: seasonal behavior, trends, and anthropogenic influence. *J. Geophys. Res. Atmos.* 90, 10463–10482. doi:10.1029/jd090id06p10463
- Ma, Z., Hu, X., Huang, L., Bi, J., and Liu, Y. (2014). Estimating ground-level PM<sub>2.5</sub> in China using satellite remote sensing. *Environ. Sci. and Technol.* 48, 7436–7444. doi:10.1021/es5009399
- MacDonald, E., and Rang, S. (2007). Exposing Canada's Chemical Valley: an investigation of cumulative air pollution emissions in the Sarnia, Ontario area.
- Makar, P., Zhang, J., Gong, W., Stroud, C., Sills, D., Hayden, K., et al. (2010). Mass tracking for chemical analysis: the causes of ozone formation in southern Ontario during BAQS-Met 2007. *Atmos. Chem. Phys.* 10, 11151–11173. doi:10.5194/acp-10-11151-2010
- McGuire, M., Jeong, C.-H., Slowik, J., Chang, R. Y. W., Corbin, J., Lu, G., et al. (2011). Elucidating determinants of aerosol composition through particle-type-based receptor modeling. *Atmos. Chem. Phys.* 11, 8133–8155. doi:10.5194/acp-11-8133-2011
- Mills, G., Pleijel, H., Malley, C. S., Sinha, B., Cooper, O. R., Schultz, M. G., et al. (2018). Tropospheric Ozone Assessment Report: present-day tropospheric ozone distribution and trends relevant to vegetation. *Elem. Sci. Anthropocene* 6 (47). doi:10.1525/elementa.302
- Ministry of the Environment and Climate Change (2018a). *Air quality in ontario 2016 report*. Ontario.
- Ministry of the Environment and Climate Change (2018b). *Air quality in ontario 2017 report*. Ontario.
- Ministry of the Environment and Climate Change (2018c). *Air quality in ontario 2018 report*. Ontario.
- Ministry of the Environment and Climate Change (2019). *Air quality in ontario 2019 report*. Ontario.
- Ministry of the Environment and Climate Change (2020). *Air quality in ontario 2020 report*. Ontario.
- Ministry of the Environment and Climate Change (2021). *Air quality in ontario 2021 report*. Ontario.
- Ministry of the Environment and Climate Change (2022). *Air quality in ontario 2022 report*. Ontario.
- Miyazaki, K., Bowman, K. W., Yumimoto, K., Walker, T., and Sudo, K. (2020). Evaluation of a multi-model, multi-constituent assimilation framework for tropospheric chemical reanalysis. *Atmos. Chem. Phys.* 20, 931–967. doi:10.5194/acp-20-931-2020
- Monks, P. S. (2000). A review of the observations and origins of the spring ozone maximum. *Atmos. Environ.* 34, 3545–3561. doi:10.1016/s1352-2310(00)00129-1
- Muñoz-Sabater, J., Dutra, E., Agustí-Panareda, A., Albergel, C., Arduini, G., Balsamo, G., et al. (2021). ERA5-Land: a state-of-the-art global reanalysis dataset for land applications. *Earth Syst. Sci. data* 13, 4349–4383. doi:10.5194/essd-13-4349-2021
- Oltmans, S. J., Lefohn, A. S., Harris, J., Galbally, I., Scheel, H., Bodeker, G., et al. (2006). Long-term changes in tropospheric ozone. *Atmos. Environ.* 40, 3156–3173. doi:10.1016/j.atmosenv.2006.01.029
- Parrish, D. D., Law, K. S., Staehelin, J., Derwent, R., Cooper, O. R., Tanimoto, H., et al. (2012). Long-term changes in lower tropospheric baseline ozone concentrations at northern mid-latitudes. *Atmos. Chem. Phys.* 12, 11485–11504. doi:10.5194/acp-12-11485-2012
- Penkett, S., and Brice, K. (1986). The spring maximum in photo-oxidants in the Northern Hemisphere troposphere. *Nature* 319, 655–657. doi:10.1038/319655a0
- Rahpoe, N., Weber, M., Rozanov, A., Weigel, K., Bovensmann, H., Burrows, J., et al. (2015). Relative drifts and biases between six ozone limb satellite measurements from the last decade. *Atmos. Meas. Tech.* 8, 4369–4381. doi:10.5194/amt-8-4369-2015
- Reid, N., Yap, D., and Bloxam, R. (2008). The potential role of background ozone on current and emerging air issues: an overview. *Air Qual. Atmos. and Health* 1, 19–29. doi:10.1007/s11869-008-0005-z
- Schultz, M. G., Schröder, S., Lyapina, O., Cooper, O. R., Galbally, I., Petropavlovskikh, I., et al. (2017). Tropospheric Ozone Assessment Report: database and metrics data of global surface ozone observations. *Elem. Sci. Anthropocene* 5 (58). doi:10.1525/elementa.244
- Shen, L., and Mickley, L. J. (2017). Seasonal prediction of US summertime ozone using statistical analysis of large scale climate patterns, *Proc. Natl. Acad. Sci. U. S. A.*, 114, 2491–2496. doi:10.1073/pnas.1610708114
- Singh, H. B., Ludwig, F. L., and Johnson, W. B. (1978). Tropospheric ozone: concentrations and variabilities in clean remote atmospheres. *Atmos. Environ.* 12, 2185–2196. doi:10.1016/0004-6981(78)90174-9
- Tai, A. P., Mickley, L. J., and Jacob, D. J. (2010). Correlations between fine particulate matter (PM<sub>2.5</sub>) and meteorological variables in the United States: implications for the sensitivity of PM<sub>2.5</sub> to climate change. *Atmos. Environ.* 44, 3976–3984. doi:10.1016/j.atmosenv.2010.06.060
- Vieira, I., Verbeeck, H., Meunier, F., Peaucelle, M., Sibret, T., Lefevre, L., et al. (2023). Global reanalysis products cannot reproduce seasonal and diurnal cycles of tropospheric ozone in the Congo Basin. *Atmos. Environ.* 304, 119773. doi:10.1016/j.atmosenv.2023.119773
- Vingarzan, R. (2004). A review of surface ozone background levels and trends. *Atmos. Environ.* 38, 3431–3442. doi:10.1016/s1352-2310(04)00280-8
- Wang, Y., Yang, Y., Yuan, Q., Li, T., Zhou, Y., Zong, L., et al. (2025). Substantially underestimated global health risks of current ozone pollution. *Nat. Commun.* 16, 102. doi:10.1038/s41467-024-55450-0
- Wang, Y., Yuan, Q., Li, T., Zhu, L., and Zhang, L. (2021). Estimating daily full-coverage near surface O<sub>3</sub>, CO, and NO<sub>2</sub> concentrations at a high spatial resolution over China based on S5P-TROPOMI and GEOS-FP. *ISPRS J. Photogrammetry Remote Sens.* 175, 311–325. doi:10.1016/j.isprsjprs.2021.03.018
- Wei, J., Li, Z., Lyapustin, A., Sun, L., Peng, Y., Xue, W., et al. (2021). Reconstructing 1-km-resolution high-quality PM<sub>2.5</sub> data records from 2000 to 2018 in China: spatiotemporal variations and policy implications. *Remote Sens. Environ.* 252, 112136. doi:10.1016/j.rse.2020.112136

- WHO (2023). WHO ambient air quality database, 2022 update: status report. *World Health Organization* 2023.
- Yan, X., Zang, Z., Li, Z., Chen, H. W., Chen, J., Jiang, Y., et al. (2024). Deep learning with pretrained framework unleashes the power of satellite-based global fine-mode aerosol retrieval. *Environ. Sci. and Technol.* 58, 14260–14270. doi:10.1021/acs.est.4c02701
- Yan, X., Zuo, C., Li, Z., Chen, H. W., Jiang, Y., He, B., et al. (2023). Cooperative simultaneous inversion of satellite-based real-time PM2.5 and ozone levels using an improved deep learning model with attention mechanism. *Environ. Pollut.* 327, 121509. doi:10.1016/j.envpol.2023.121509
- Yang, L., Luo, H., Yuan, Z., Zheng, J., Huang, Z., Li, C., et al. (2019). Quantitative impacts of meteorology and precursor emission changes on the long-term trend of ambient ozone over the Pearl River Delta, China, and implications for ozone control strategy. *Atmos. Chem. Phys.* 19, 12901–12916. doi:10.5194/acp-19-12901-2019
- Young, P. J., Naik, V., Fiore, A. M., Gaudel, A., Guo, J., Lin, M., et al. (2018). Tropospheric Ozone Assessment Report: assessment of global-scale model performance for global and regional ozone distributions, variability, and trends. *Elem. Sci. Anthropocene* 6 (10). doi:10.1525/elementa.265
- Zang, Z., Guo, Y., Jiang, Y., Zuo, C., Li, D., Shi, W., et al. (2021). Tree-based ensemble deep learning model for spatiotemporal surface ozone ( $O_3$ ) prediction and interpretation. *Int. J. Appl. Earth Observation Geoinformation* 103, 102516. doi:10.1016/j.jag.2021.102516